Constraints on Moho depth and crustal thickness in the Liguro-Provençal basin from a 3D gravity inversion: geodynamic implications

N. CHAMOT-ROOKE[1], J.-M. GAULIER[2] & F. JESTIN[1]

[1]Laboratoire de Géologie, CNRS-URA 1316, Ecole Normale Supérieure, 24 rue Lhomond, 75231 Paris Cedex 05, France (e-mail: rooke@sphene.ens.fr)

[2]Institut Français du Pétrole, Geology & Geochemistry Division, 1 & 4 av Bois-Préau, BP311, 92506 Rueil Malmaison Cedex, France

Present address: Beicip Franlab, 232 avenue Napoléon Bonaparte, 92 500 Rueil Malmaison, France

Abstract: 3D gravity modelling is combined with seismic refraction and reflection data to constrain a new Moho depth map in the Liguro-Provençal basin (Western Mediterranean Sea). At seismically controlled points, the misfit between the gravimetric solution and the seismic data is about 2 km for a range of Moho depths between 12 km (deep basin) and 30 km (mainland). The oceanic crust thickness in the deep basin (5 km) is smaller than the average oceanic crust thickness reported in open oceans (7 km), pointing to a potential mantle temperature 30–50°C below normal and/or very slow oceanic spreading rate. Oceanic crust thickness is decreasing towards the Ligurian Sea and towards the continent–ocean boundary to values as small as 2 km. Poor magma supply is a result of low potential mantle temperature at depth, lateral thermal conduction towards an unextended continental margin, and decrease of the oceanic spreading rate close to the pole of opening in the Ligurian Sea. Re-examination of magnetic data (palaeomagnetic data and magnetic lineations) indicates that opening of the Liguro-Provençal Basin may have ceased as late as Late Burdigalian time (16.5 Ma) or even later. The absence of a significant time gap between cessation of opening in the Liguro-Provençal Basin and rifting of the Tyrrhenian domain favours a continuous extension mechanism since late Oligocene time driven by the African trench retreat.

Determination of the deep structure across continental margins has been one of the major goals achieved through deep seismic profiling in recent years. Two kinds of deep-seismic soundings have been obtained so far across the Gulf of Lion margin and adjacent deep basin: multichannel seismics of ECORS type and wide-angle refraction data using the two-ship expanding spread profile technique. Both techniques are complementary, since multichannel profiles image the main structures along a section of the basin, from the surface to Moho depth, while ESPs constrain the 1D velocity structure at some spots along the section. Deep-reflection and refraction techniques were particularly successful in reaching the crust–mantle discontinuity (Moho) in the Gulf of Lion area. However, seismic data remain sparse. Variability of the crustal structure is high, both across the margins (from unstretched continental crust to oceanic crust) and along (for instance from smoothly stretched Gulf of Lion margin to sharply stretched Provençal margin). The oceanic crust thickness in the deeper part of the basin is also highly variable. The deep structure of the basin is thus complex, preventing reliable extrapolation from sparse seismic data.

Gravity data can be used to obtain a reliable geometry of the Moho discontinuity in regions where no further information is available. The triangular shape of the Liguro-Provençal Basin requires 3D gravity inversion. The use of Fourier transforms to invert for the shape of the Moho is briefly described. Seismic Moho data are then used to determine free parameters in the inversion and to control the validity of the gravimetric solution. The new Moho depth and crustal thickness maps are finally used to discuss some of the geodynamic implications.

Establishing a new Moho depth map from 3D gravity inversion

Seismic Moho depth data

Moho depth data are sparsely available in the Gulf of Lion and surrounding areas. Continental refraction data indicate an average Moho depth of 30–32 km on the mainland (southern Rhône valley, Sapin & Hirn 1974; Spanish mainland,

CHAMOT-ROOKE, N., GAULIER, J.-M. & JESTIN, F. 1999. Constraints on Moho depth and crustal thickness in the Liguro-Provençal basin from a 3D gravity inversion: geodynamic implications. *In:* DURAND, B., JOLIVET, L., HORVÁTH, F. & SÉRANNE, M. (eds) *The Mediterranean Basins: Tertiary Extension within the Alpine Orogen.* Geological Society, London, Special Publications, **156,** 37–61.

Zeyen *et al.* 1985; Danobeitia *et al.* 1992). Moho depth increases to 60–65 km beneath the Pyrénées belt (Choukroune & Team 1989; Choukroune *et al.* 1990; Anguy *et al.* 1991) and to 55–60 km beneath the Alps (Giese *et al.* 1973). Beneath the Balearic Islands the Moho lies at an average depth of 22 km (18 km under Menorca according to Banda *et al.* 1980; 24–28 km under Mallorca according to Danobeitia *et al.* 1992). The Moho is slightly deeper beneath Corsica and Sardinia (average 30 km depth, Egger *et al.* 1988; Egger 1992).

At sea, both refraction and reflection data are available. Based on Expanding Spread Profiles (ESPs) the average Moho depth in the Liguro-Provençal basin and in the Valencia Trough is 15 km (Le Douaran *et al.* 1984; Gallart *et al.* 1980; Danobeitia *et al.* 1992; Mauffret *et al.* 1992, 1995; Pascal *et al.* 1992, 1993; Torné *et al.* 1992). The Liguro-Provençal Basin is floored with thin oceanic crust of early Miocene age (Bayer *et al.* 1973; Burrus 1984), whereas thin continental crust underlies the Valencia Trough (Watts & Torné 1992*a*, *b*; Pascal *et al.* 1992). Progressive thinning of the continental crust from the upper margin to the deeper basin is clearly evidenced over the Gulf of Lion margin through subsidence analysis (Steckler & Watts 1980) and multichannel deep seismic profiling (ECORS profiles, de Voogd *et al.* 1991). The exact position of the ocean–continent boundary is, however, still debated (e.g. Pascal *et al.* 1993; Mauffret *et al.* 1995; review in Vially & Trémolières 1996).

The non-uniform data distribution precludes the use of standard interpolation to recover a complete Moho depth map. We thus briefly describe in the following section the use of gravity data to constrain better the Moho depth map where no other information is available.

3D gravity inversion procedure

The 3D inversion procedure is based on Fourier transform (FT) methods (Parker 1973), using the first-order theory in which high-order terms in the gravity expansion are being neglected. The gravity anomaly at the Earth's surface due to a periodic undulation $h(x,y)$ of an interface at depth d associated with a constant density contrast $\Delta\rho$ is thus given by

$$\Delta g(x,y) = 2\pi G \Delta\rho h(x,y) e^{-kd} \quad (1)$$

where k is the wavenumber of the undulation ($k = 2\pi/\lambda$, where λ is the wavelength) and G is the universal gravity constant. Fourier transforming this equation leads to

$$\Delta g^*(k_x,k_y) = 2\pi G \Delta\rho h^*(k_x,k_y) e^{-kd} \quad (2)$$

where $\Delta g^*(k_x,k_y)$ and $h^*(k_x,k_y)$ denote the 2D Fourier transform of the gravity signal and of the undulations, respectively (k_x and k_y are the horizontal wavenumbers in x and y directions). $h^*(k_x,k_y)$ can thus be obtained by Fourier transforming the gravity signal as

$$h^*(k_x,k_y) = 1/(2\pi G \Delta\rho) \Delta g^*(k_x,k_y) e^{kd} \quad (3)$$

Inverse FT finally leads to $h(x,y)$.

Exponential terms in equation 3 at high wavenumbers (short wavelengths) require filters to smooth the observed data prior to inversion. We tested a number of filters in the spectral domain by using forward and inverse modelling. Best results were obtained using gaussian or cosine filters to attenuate short wavelengths before applying the inverse FT. Such filters also minimizes the side-lobe effects inherent to FT methods. A cosine filter cutting all wavelengths shorter than 60 km was used in the final solutions.

The method applies to a single interface with known reference level (d) and density contrast ($\Delta\rho$). We show in the next section how we derived a mantle Bouguer gravity anomaly to perform the inversion on the Moho discontinuity, and how we adjusted the reference level and crust–mantle density contrast.

Mantle bouguer in the Liguro-Provençal Basin

Bathymetry and topography were taken from the International Bathymetric Chart of the Mediterranean (IBCM) and from the ETOPO5 digital data files respectively. A single sedimentary layer from sea bottom to top of basement is used. The basement depth map was compiled from Arthaud *et al.* (1980) for the Oligocene sedimentary basins offshore, a digital data file from Mauffret (pers. comm.) and Gorini (1993) for the Gulf of Lion, Réhault (1981) for the Ligurian Sea and surrounding areas, Maillard *et al.* (1992) for the Valencia Trough, Moussat (1983) and Réhault *et al.* (1987) for the Tyrrhenian Sea, Réhault *et al.* (1984) for the remaining areas. Data were compiled in seismic two-way travel time. Velocities at ESP reprocessed by Pascal *et al.* (1993) were then used for time to depth conversions.

Gravity maps were derived from the IBCM Bouguer anomaly maps. Since in the oceanic domain a simple Bouguer approximation with a density of 2670 kg m^{-3} was used in the IBCM charts, we first recalculated the corresponding free-air anomaly with the bathymetry also provided by IBCM. The obtained free-air anomaly

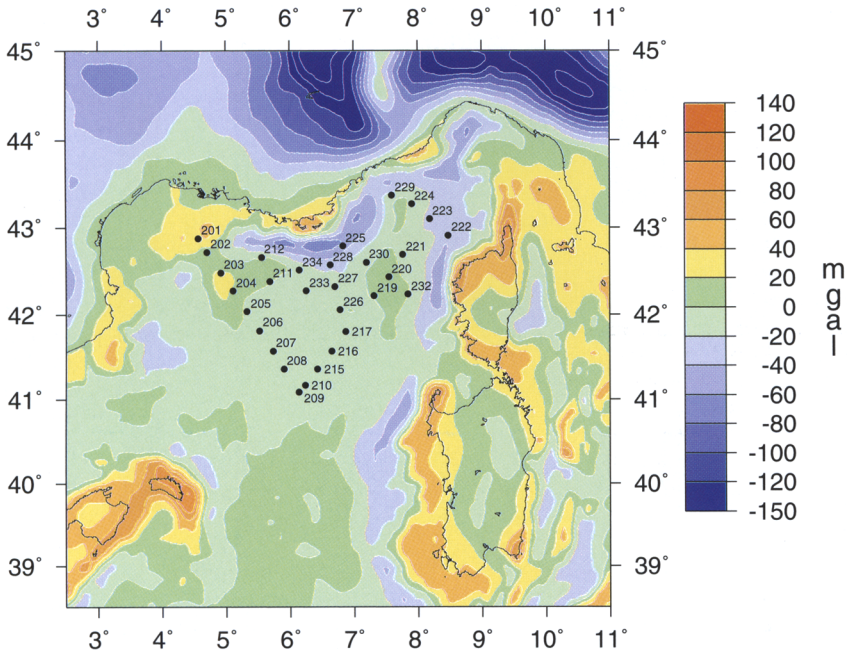

Fig. 1. Free-air anomaly map in the Liguro-Provençal basin. On land: Bouguer anomaly from the IBCM charts (Bouguer density 2.67). Contour interval: 20 mgal.

map (Fig. 1) was compared to two other sources of data: individual free-air gravity profiles extracted from the GEOMAR data base and satellite-derived gravity field of Sandwell (Sandwell & Smith 1995). At wavelengths greater than 15 km the IBCM ship-derived map does not differ significantly from the satellite gravity map. The latter has, however, a much better resolution due to continuous cover as opposed to non-uniform ship-track coverage.

The final mantle Bouguer anomaly map was obtained by correcting the free air anomaly for water and sediment, both being replaced by crust (Fig. 2). This was done by calculating their respective gravity contribution using contouring and summing up individual thin (100 m thick) sheet contributions in 3D (Talwani & Ewing 1960). Notice that at this stage, Fourier domain gravity expansion was not used. 3D marine Bouguer anomaly maps (replacing water by sediment) were also produced.

Reference level and crust-mantle density contrast

The mantle Bouguer gravity anomaly can be attributed to Moho undulations to a first approximation. The possible contribution of deeper sources, in particular the effect of laterally variable thermal and crustal density structure, will be discussed in a later section. If we consider topography of the Moho as the only gravitational source remaining, then the previous inversion methodology applies. Free parameters in the gravity inversion are the reference level (depth d) and the density contrast of the crust–mantle boundary ($\Delta\rho$). Uncertainties, apart from the oversimplified sedimentary column, arise from the choice of the mean sediment density and crustal density used to calculate the mantle Bouguer. The best couple of parameters d and $\Delta\rho$ was determined by minimizing by least squares fit the difference between the calculated Moho depth and the observed seismic Moho depth.

Results for d and $\Delta\rho$ best couple are displayed in Fig. 3, and seismic Moho depth and gravimetric Moho depth are compared in Table 1. We tested the influence of sediment and crust density in the ranges 2200–2350 kg m^{-3} and 2750–2800 kg m^{-3} respectively. Quality of the fit is rather insensitive to densities, with a standard deviation of 2300 m for all runs at refraction and reflection control points (mean misfit between seismic and gravimetric Moho depths). Standard

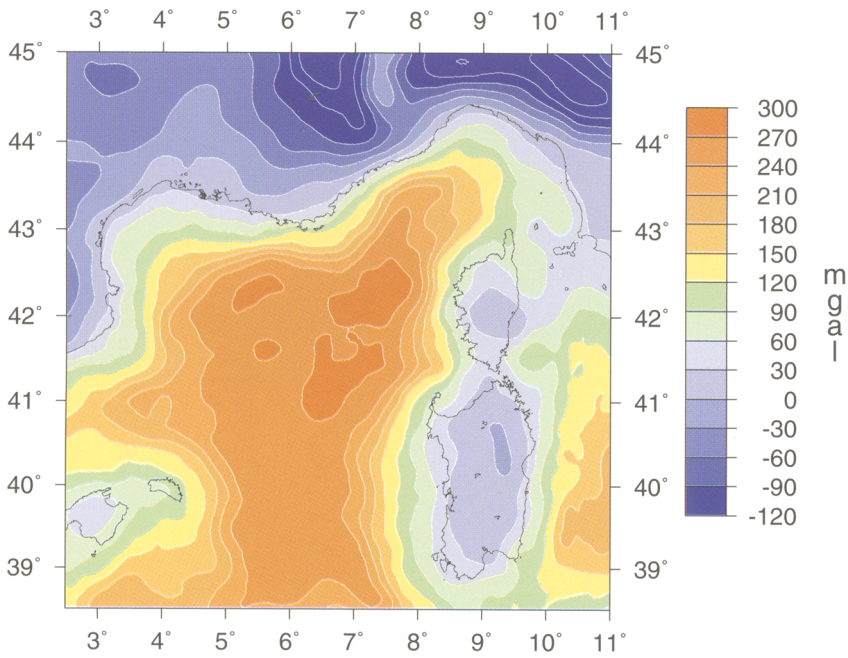

Fig. 2. Mantle Bouguer anomaly map (Model A solution; no thermal correction nor variable crust density correction). Contour interval: 30 mgal.

deviation for ESP points only (oceanic domain) reduces to 1500 m for the same runs. In all cases the best reference level was found close to 27–28 km. Varying the sediment density or the crust density is merely accommodated by a modification of the $\Delta\rho$ contrast at the crust–mantle interface: $\Delta\rho$ is increasing with decreasing sediment density (Fig. 3d) and/or increasing crust density (Fig. 3c) . A reasonable $\Delta\rho$ contrast of 580 kg m^{-3} was obtained for a mean sediment density of 2350 kg/m^{-3} and a crustal density of 2750 kg m^{-3}, thus giving a mantle density of 3330 kg m^{-3}. This model is referred to as Model A in the following discussions (Fig. 4a).

Fourier domain expression for gravity requires the reference level to be the median depth of the interface in order to optimize convergence of the series expansion (Parker 1973; Cowie & Karner 1990). The same limitation applies for the first-order theory used here (non-zero first term only), so that the solution will only be approximate if the median depth of the interface is different from the reference level. The reference level found through the inversion process (27–28 km) is actually deeper than the *a posteriori* calculated mean depth of the interface (25 km). The corresponding error in the calculated gravity is a function of the wavelengths of the anomalies through the exponential term in equation 1, the error decreasing with increasing wavelength. The validity of the final solution was checked by calculating the true 3D Bouguer (using the discrete sum of thin sheet contributions, Talwani & Ewing 1960). The standard deviation of the residual (observed minus modelled, Fig. 5) is 15 mgal, or 600 m translated into depth of the Moho. Typical misfit reaches 20 mgal on the margins and 10 mgals in the deeper parts of the basin. The misfit is high towards the sides of the box due to the outside box apodization prior to Fourier inversion. At that point, the obtained solution could easily be improved by re-introducing short wavelengths as small perturbations of the Moho.

Fig. 3. Reference Moho depth (d) and mantle–crust density contrast ($\Delta\rho$) best couple obtained by least squares minimization at seismic control points (standard deviation s.d. in km). (**a**) Model A solution (no thermal nor variable crust density corrections; d = 27.7 km and $\Delta\rho$ = 580 kg m^{-3}). (**b**) Model B solution (includes thermal and variable crust density corrections). (**c**) Effect of crust density increase. (**d**) Effect of sediment density decrease.

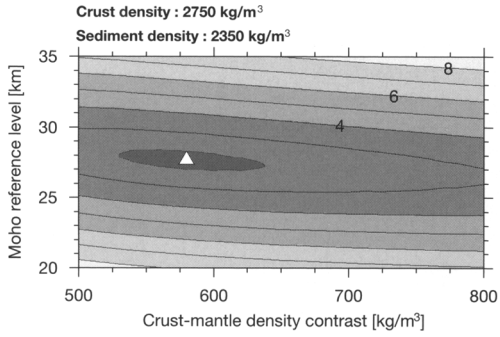

Best fit information:
Moho reference level : 27.7 km
$\Delta\rho$: 580 kg/m^3
s.d. : 2.31 km

a

MODEL A
No thermal correction

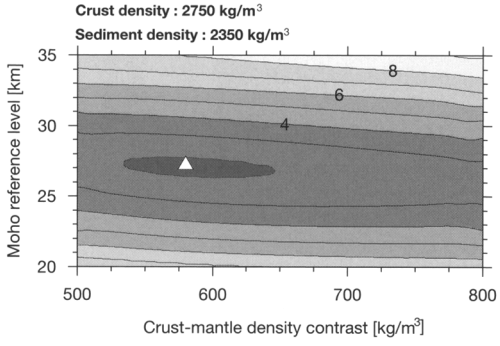

Best fit information:
Moho reference level : 27.2 km
$\Delta\rho$: 580 kg/m^3
s.d. : 1.98 km

b

MODEL B
With thermal correction

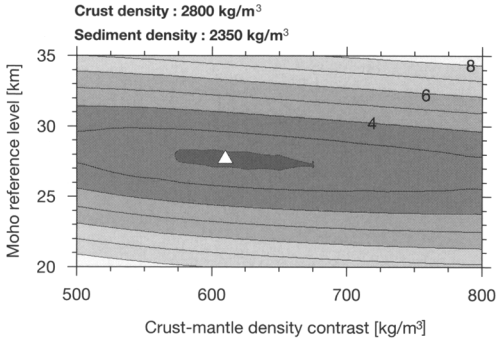

Best fit information:
Moho reference level : 27.7 km
$\Delta\rho$: 610 kg/m^3
s.d. : 2.31 km

c

Increased crust density
No thermal correction

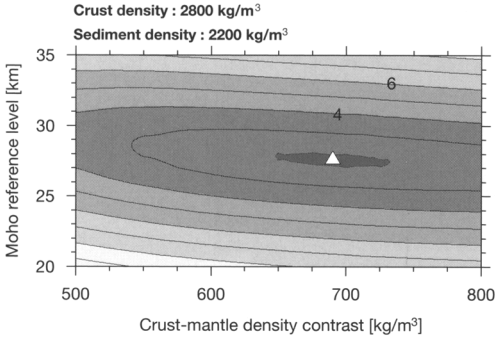

Best fit information:
Moho reference level : 27.6 km
$\Delta\rho$: 690 kg/m^3
s.d. : 2.35 km

d

Decreased sediment density
No thermal correction

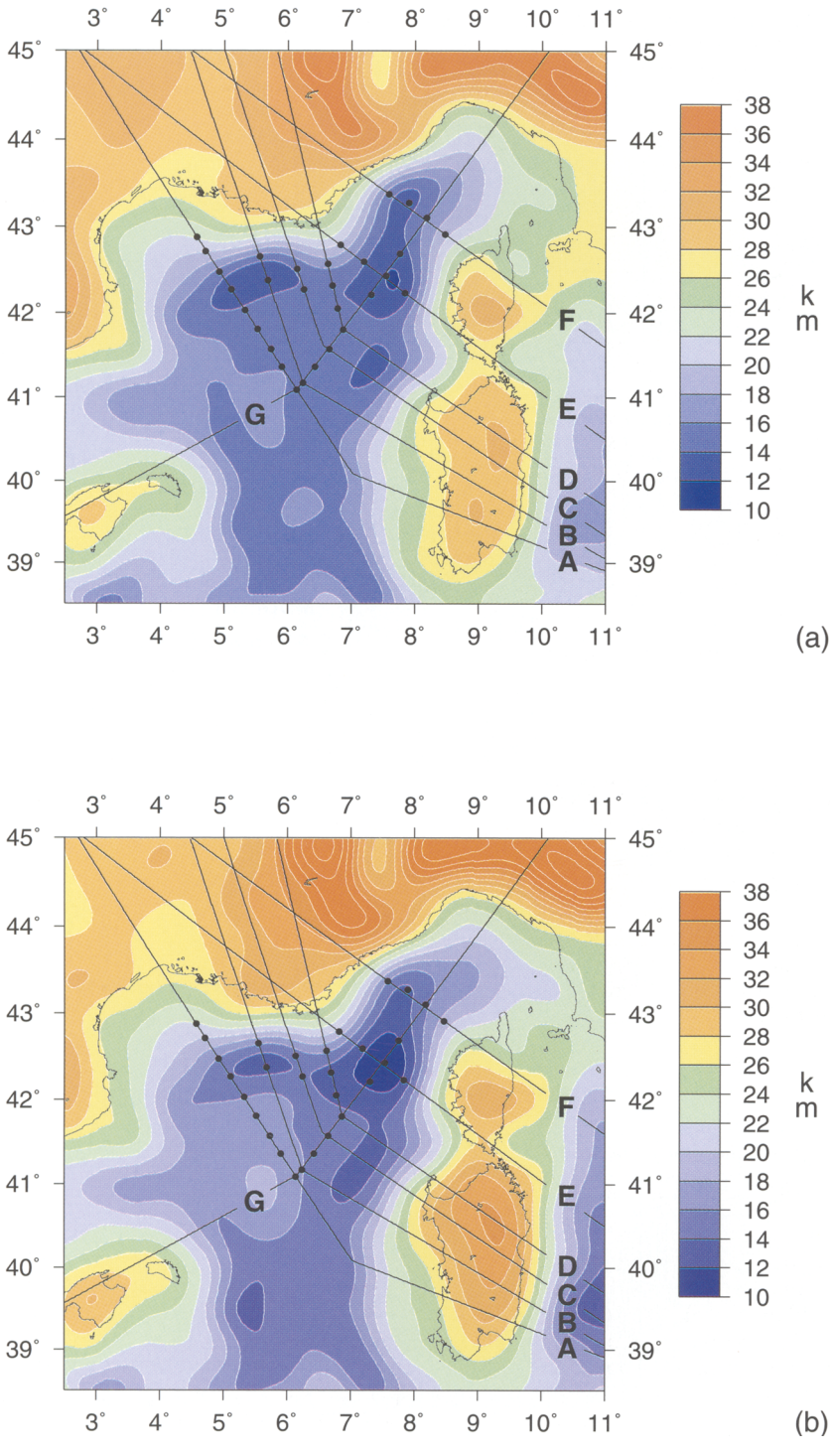

Fig. 4. Results of the 3D gravity inversion (depth to Moho contoured every 2 km). (**a**) Model A solution. (**b**) Model B solution. Location of seismic control points are shown as open dots. Sections A, B, C, D, E, F and G run across ESP data points at sea.

Table 1. *Comparison between seismic Moho depth and gravimetric Moho depth at ESP control points (for both Model A and Model B solutions)*

Lat N		Long E		ESP no.	Seismic Moho (km)	Model A (km)	Misfit (km)	Model B (km)	Misfit (km)
(°)	(′)	(°)	(′)						
42	53	4	34	ESP201	19.9	22.2	–2.3	21.9	–2.0
42	43	4	43	ESP202	19.8	20.2	–0.4	20.1	–0.3
42	29	4	55	ESP203	15.1	15.4	–0.3	16.1	–1.0
42	16	5	7	ESP204	14.8	13.0	1.8	14.2	0.5
42	2	5	20	ESP205	14.2	14.3	–0.1	15.9	–1.7
41	49	5	31	ESP206	15.1	14.9	0.2	16.5	–1.4
41	34	5	44	ESP207	14.7	15.1	–0.4	16.4	–1.7
41	22	5	54	ESP208	15.5	15.9	–0.4	17.1	–1.6
41	5	6	8	ESP209	15.3	15.4	–0.1	16.7	–1.4
41	10	6	14	ESP210	15.0	15.2	–0.2	16.1	–1.1
42	23	5	41	ESP211	14.6	12.6	2.0	13.4	1.2
42	40	5	33	ESP212	13.3	15.4	–2.1	16.2	–2.9
41	22	6	26	ESP215	15.0	15.0	0.0	15.4	–0.4
41	34	6	39	ESP216	15.3	15.1	0.2	15.1	0.1
41	48	6	52	ESP217	14.0	15.0	–1.0	14.5	–0.5
42	13	7	19	ESP219	13.0	13.1	–0.1	11.5	1.5
42	26	7	32	ESP220	12.5	12.0	0.5	10.4	2.1
42	41	7	46	ESP221	13.0	13.1	–0.1	11.9	1.1
42	55	8	28	ESP222	15.5	19.4	–3.9	18.6	–3.1
43	6	8	11	ESP223	14.0	16.0	–2.0	15.5	–1.5
43	16	7	54	ESP224	13.0	13.3	–0.3	13.7	–0.7
42	47	6	49	ESP225	22.0	19.6	2.4	19.1	2.9
42	3	6	47	ESP226	14.0	14.4	–0.4	13.4	0.6
42	19	6	42	ESP227	14.5	14.3	0.2	13.2	1.3
42	34	6	37	ESP228	20.5	16.8	3.7	16.2	4.3
43	22	7	35	ESP229	15.5	15.1	0.4	16.0	–0.5
42	36	7	11	ESP230	12.0	14.2	–2.2	12.5	–0.5
42	14	7	50	ESP232	13.0	13.1	–0.1	12.5	0.5
42	16	6	15	ESP233	13.5	14.3	–0.8	14.2	–0.7
42	31	6	8	ESP234	13.0	14.5	–1.5	14.8	–1.8
41	4	3	41	ESP002	14.5	16.9	–2.4	17.6	–3.1
							s.d. 1.52		s.d. 1.72

Model A: no thermal and no variable crust cdensity corrections.
Model B: thermal and variable crust density included.
s.d. is standard deviation in km.

Thermal, variable crust density and variable sediment density corrections

The observed heat flow in the Liguro-Provençal basin is high (Fig. 6a). Values corrected for thermal blanketing are mostly above 100 mW m^{-2} and reach 140–160 mW m^{-2} in the axial part of the basin, based on the recent EGT heat flow compilation (European Geotraverse, Della Vedova *et al.* 1995). High heat flow anomaly in the basin is a consequence of the Oligocene rifting and the following short period of oceanic accretion. The net effect of the positive thermal anomaly in the basin is to reduce the mantle density at depth, producing a negative contribution of several tens of mgal to the gravity field (Watts & Torné 1992*a*, *b*).

To include this correction in the calculation of the mantle Bouguer, we modelled two sections across the basin: a Gulf of Lion section (section B located in Fig. 4) and a Ligurian section (section E located in Fig. 4). The temperature field was calculated following a pure shear McKenzie-type model for the rifting period (30–23 Ma), including lateral heat conduction and finite rifting duration (Alvarez *et al.* 1984), and oceanic accretion for the spreading period (23–19 Ma). Thermal cooling by conduction was assumed from 19 Ma to present. Ages are taken from quantitative subsidence analysis of Bessis

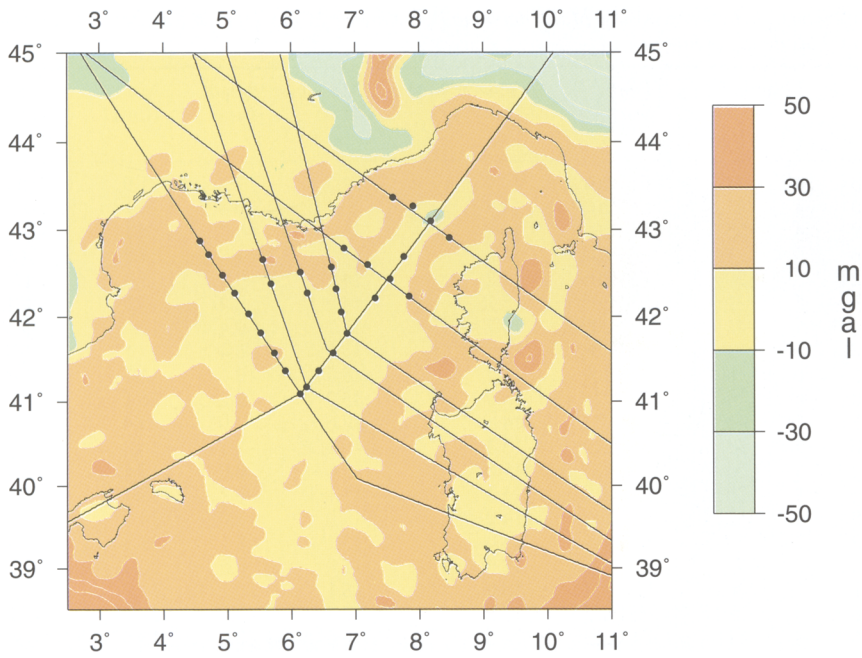

Fig. 5. Residual Bouguer (observed minus modelled) using Model A solution and 3D analytic calculations (thin sheets summation).

(1986) and Burrus (1989). The crustal structure used as input was derived from the Model A solution. Finally, the thermal anomaly was converted to a density anomaly to obtain the corresponding gravity field through 2D gravity modelling (Fig. 7).

The result of the 2D thermal/gravity modelling is that the anomalous gravity field can be directly obtained with a reasonable accuracy by simply multiplying in the Fourier domain the anomalous surface heat flow with an exponential function of Fourier gravity type (Fig. 7, top):

$$\Delta g^*(k_x,k_y) = A\ \Delta\phi^*(k_x,k_y)\ e^{-k D} \qquad (4)$$

where $\Delta g^*(k_x,k_y)$ is the gravity anomaly associated with the anomalous heat flow $\Delta\phi^*(k_x,k_y)$, and A and D are function parameters. Notice that D has the dimension of a distance and can be viewed as the mean depth of the thermal disturbance. Parameters A and k integrate the geometry and amplitude of the thermal anomaly. Parameters A and D were found to be quite similar for the two sections modelled (A in the range 2.95–3.04 10^{-2} m^3 s^{-2} W^{-1} and $D = 50 \pm 3$ km). Mean A and D values were thus applied to the thermal anomaly heat flow map to get a 3D estimate of the gravity contribution. The results are shown in Fig. 6b. The negative thermal contribution to the gravity field is maximum in the axial part of the Liguro-Provençal basin, towards the Ligurian Sea, where the gravity effect reaches –50 mgal. This is significantly less than the gravity effect calculated in 2D (–65 mgal and –110 mgal for sections B and E respectively) indicating that 2D modelling would overestimate the thermal correction. Notice that highest heat flow values were measured in the Ligurian Sea, rather than the central part of the basin as would be predicted. We attribute the low values of the central part of the basin to the blanketing effect of the Rhone delta deposits.

A second type of correction is related to the lateral variations of the density of the crust. The density of the oceanic crust is known to be greater than the mean density of the continental crust. The contribution to the gravity field is opposite to the previous thermal correction since it implies a positive gravity anomaly over the oceanic domain. An estimation of this contribution was obtained by calculating the difference between a mantle Bouguer at 2750 kg m^{-3} for crustal density and a mantle Bouguer at

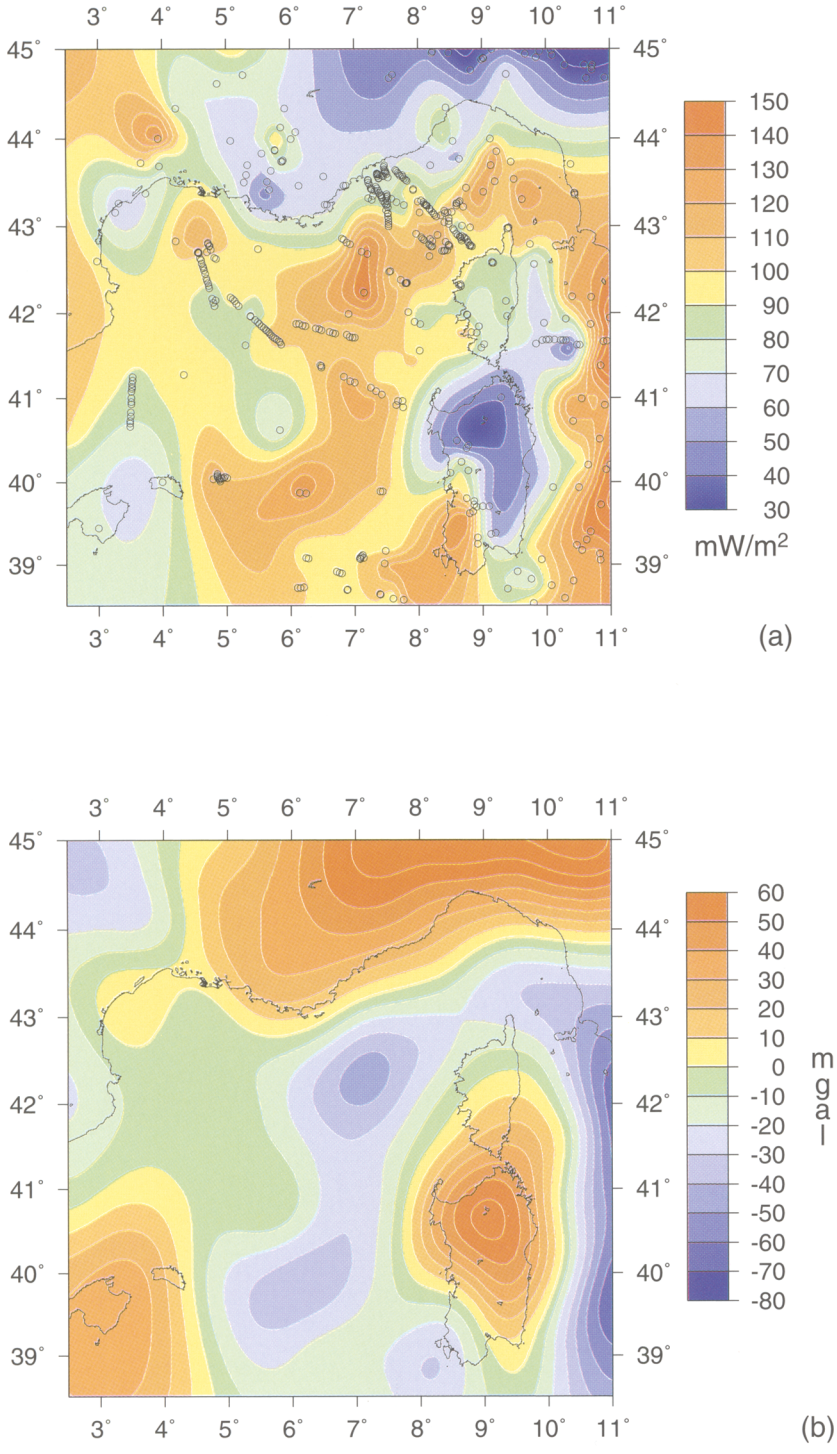

Fig. 6 (**a**) Observed heat flow (open dots: data points, from Della Vedova *et al.* 1995). Contour interval: 10 mW m^{-2}. (**b**) Calculated gravity effect of the decreasing mantle density with increasing surface heat flow. See text for details of the calculations. Contour interval: 10 mgal.

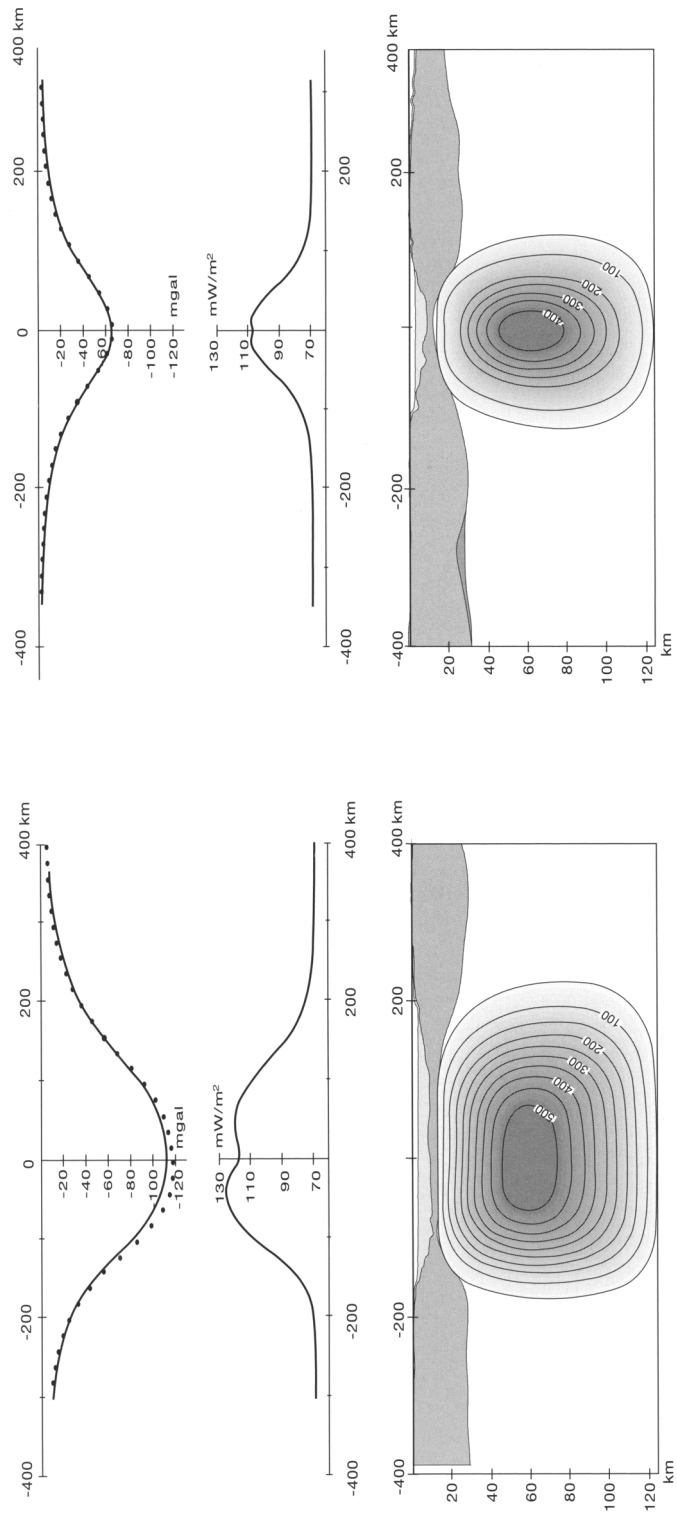

Fig. 7. Left: 2D thermal modelling along a Gulf of Lion section (section B located in Fig. 4). Right: 2D thermal modelling along a Ligurian Sea section (section E located in Fig. 4).

Bottom: Remaining present-day temperature anomaly following Oligo-Miocene rifting and oceanic accretion. Pure shear extension model is assumed. Contour interval: 50°C. Middle: Computed surface heat flow. Top: Continuous curve: gravity signal induced by the thermal anomaly, calculated analytically using polygonal bodies. Dotted points: gravity signal directly calculated from the surface heat flow by means of Fourier transforming (see text for the details of the calculations).

2880 kg m^{-3}. The net gravity effect is reaching +40 mgal in the true oceanic domain. A similar estimate is reached if a simple Bouguer plateau approximation is calculated for a 7 km thick oceanic crust and a 130 (2880–2750) kg m^{-3} oceanic crust–continental crust density contrast.

A last type of correction deals with the gravity effect of sediment compaction. If the density of sediment is increasing with depth, which is likely to be the case in a sedimentary basin, then the uniform density model tends to overestimate sediment density on the margins and correlatively underestimate density towards the centre of the basin. The amplitude of the gravity effect depends on the density–depth function and hence on lithologies. It reaches +50 mgal in the Viking Graben (North Sea) according to Cowie & Karner (1990). Exponential-type porosity–depth functions down to about 4000 m below sea-floor are available for the Gulf of Lion margin from few industrial wells (Bessis 1986). However, compaction will not follow a simple exponential density–depth variation in the deeper part of the basin due to the thick accumulation of salt and evaporites during the Messinian. Velocity–depth functions derived from expanding spread profiles indicate high P-wave velocity (5.1–5.3 km s^{-1}) in the sediments lying immediately above the acoustic basement (Pascal *et al.* 1993). In the absence of any other information, empirical velocity–density conversion would give a 2550 kg m^{-3} density for the lowermost sediments (Nafe & Drake 1963). Using these constraints, the mean density would range from 2090 kg m^{-3}, estimated at ESP 225 where sediments are the thinnest (1900 m) to 2370 kg m^{-3}, estimated at ESP 204 where sediments are the thickest (8000 m). The net gravity effect, using a simple Bouguer plateau approximation, would reach +30 mgal, equivalent to about 1 km of Moho topography. These estimations remain, however, highly speculative in the absence of reliable depth–density data, and we did not introduce this correction further.

Corrections for thermal and oceanic crust density were applied to derive a new Moho depth map, referred as Model B (Fig. 4b). Notice that since the correction for thermal anomaly and the correction for variable crustal density are opposite in sign in the oceanic domain, Model A and Model B are quite similar there. On the mainland, negative heat flow anomaly (cold areas), such as beneath the Alps or beneath Sardinia, will tend to deepen the Moho in the gravity inversion. However, the way the gravity anomaly was derived from the heat flow is strictly valid in the oceanic domain only since homogeneous stretching followed by oceanic accretion was assumed. The quality of the fit at Moho control points is slightly enhanced in Model B with respect to Model A (standard deviation of 2000 m instead of 2300 m). However, the Model B solution degrades at ESP control points (1700 m versus 1500 m). In particular, the calculated Moho in Model B shows a systematic misfit along the ECORS profile (Table 1). This misfit is mainly resulting from the low heat-flow values, relative to surroundings, that prevail over the Gulf of Lion area.

The conclusion is that Model A (uncorrected) and Model B (corrected for variable heat-flow and variable crust density) give quite similar results. In the next section, only Model A will be considered since this solution is closer to ESP control points in the oceanic domain. We display in Fig. 8 a set of crustal sections crossing the Liguro-Provençal basin and Ligurian Sea through the refraction and reflection data points (sections are located in Fig. 4). Sections A to F are roughly perpendicular to the main structures. Section G runs obliquely from Mallorca to the Ligurian Sea and the Gulf of Genoe. Mesozoic rifting in southern France was not included in the calculations, so that the gravimetric Moho is several kilometres deeper than the seismic Moho in the Rhône graben (Section E). Apart from this discrepancy, and if we allow a standard error of 1 km on the seismically determined Moho (Pascal *et al.* 1993), the gravimetric solution fits the seismic data well.

Discussion

Variability of the oceanic crust thickness

The mean oceanic crustal thickness is close to 5.0 km. Systematic variability is, however, found both along (parallel to the magnetic lineations) and across (oceanic crust close to ocean–continent boundary) strike. The southernmost part of the Ligurian Sea (section E in Fig. 8) is floored with very thin oceanic crust (Pascal *et al.* 1993; Mauffret *et al.* 1995). At ESP 220, the Moho is rising to less than 12 km depth, which is the shallowest point of the studied area. The mean crustal thickness is 3.3 km (ESP 219, 220, 221, 230, 232) which is significantly less than the average 5.0 km thickness.

Line G (Fig. 8, bottom; located in Fig. 4) is a cross-section running SW–NE in the deep basin from the island of Mallorca to the Gulf of Genoe. This along-strike section follows more or less the axial Liguro-Provençal basin along the expected location of the fossil oceanic ridge, except for the northern end of the section. Notice the close agreement between the seismically determined

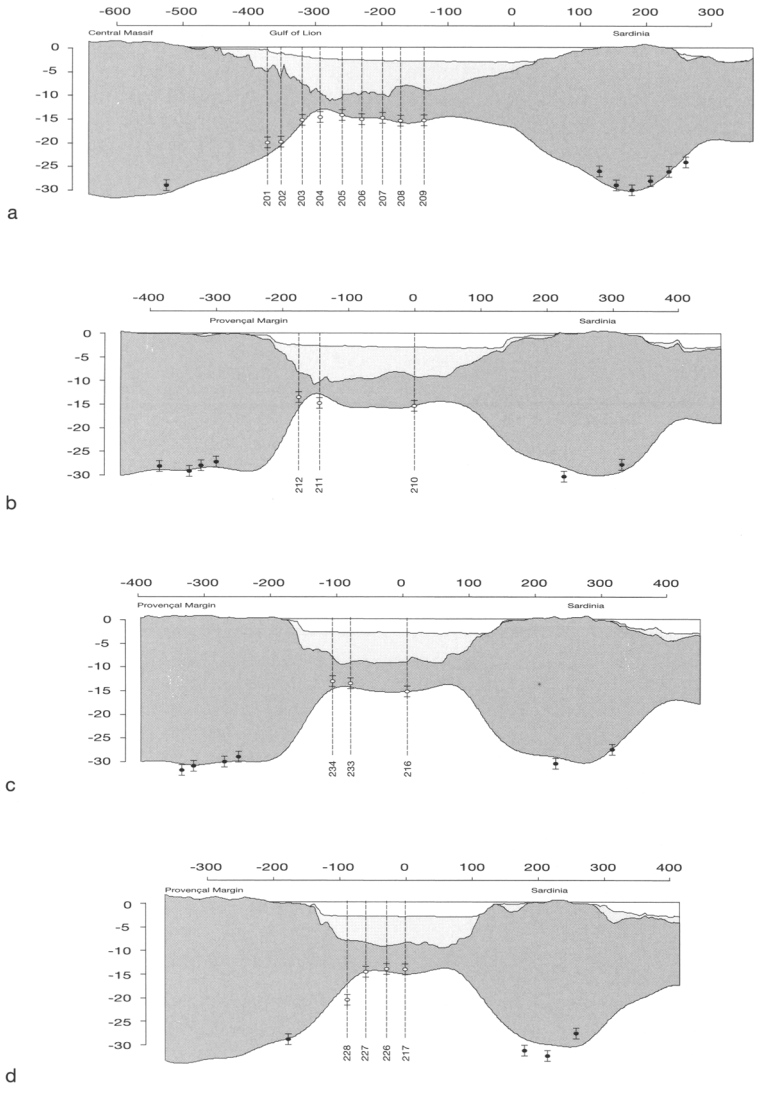

Moho and Model A gravimetric solution. Oceanic crustal thickness along the section shows a remarkable gradual decrease towards the Ligurian Sea. At ESP 210 (along the ECORS line) crustal thickness is close to 5.5 km, whereas it may be as thin as 2 km in the southernmost part of the Ligurian Sea (ESP 220).

Following pioneering works (Reid & Jackson 1981; Foucher *et al.* 1982), considerable progress has been made in the recent years on the calculations of volume of melt generated either during rifting (McKenzie & Bickle 1988; White & McKenzie 1989; Bown & White 1995*a*, *b*) or during oceanic spreading (Scott & Stevenson 1989; White *et al.* 1992; Cordery & Morgan 1993; Bown & White 1994; Su *et al.* 1994). Production of oceanic crust is a result of partial melting of the mantle as it rises beneath spreading centres. The thickness of oceanic crust is thus directly related to the amount of partial melting, in turn controlled by asthenospheric mantle temperature and lithospheric temperature field. Under moderate to normal mantle temperature conditions (range of mantle temperatures producing less than 7–8 km thick crust), all models predict a decrease of crustal thickness with

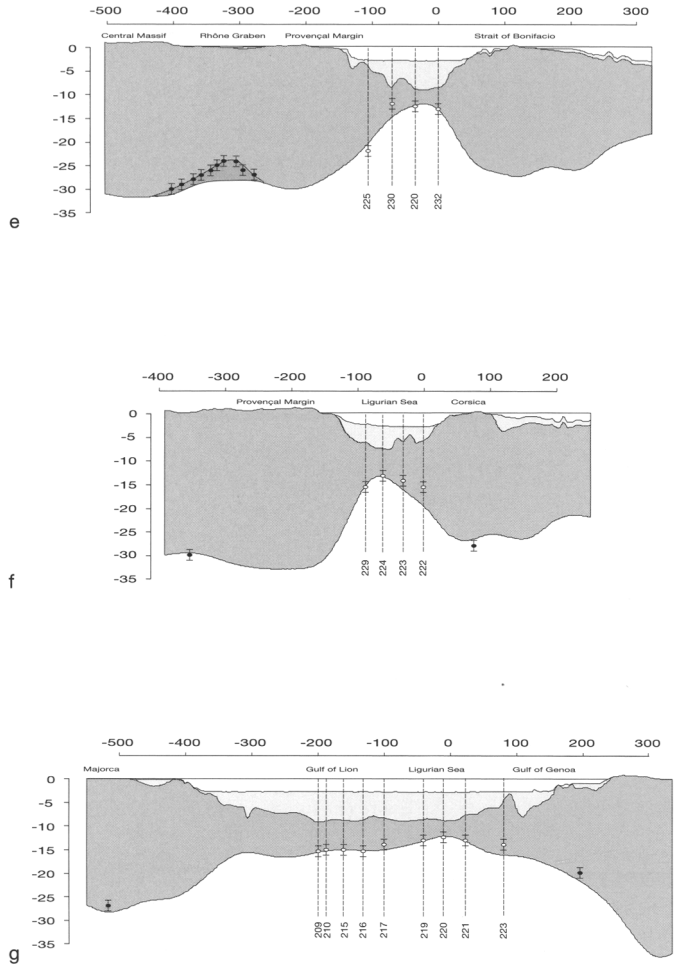

Fig. 8. Crustal sections across the Liguro-Provençal basin deduced from 3D gravity inversion (Model A solution). Open dots: ESP data points at sea (vertical bar is ± 1 km). Filled dots: reflection or refraction data points on land. Sections A to G are located in Fig. 4.

decreasing spreading rate and/or decreasing asthenospheric mantle temperature (Reid & Jackson 1981; Bown & White 1994; Su *et al.* 1994).

To explore further crustal thickness variation as a function of position in the basin, we use for each ESP the distance to the inferred Sardinia–Corsica pole of rotation (Fig. 9a & b). Different solutions have been proposed for the kinematics of the rotation (see review in Vially & Trémolières 1996). They range from simple rotation about a single pole for both rifting and spreading to more complicated solutions involving several phases. In the following we use a commonly adopted solution with a pole of rotation located in the Gulf of Genoa (N43.5°–E9.0°; Réhault *et al.* 1984). ESP data are located at distances to the pole ranging from 70 km (northernmost Ligurian Sea section) to 350 km (Gulf of Lion, ECORS section).

We show in Fig. 9a the predicted oceanic crust thickness for various potential asthenospheric mantle temperature (Bown & White 1994). Crustal thickness is given as a function of distance to the pole. We assume a 9.8° Ma^{-1} rotation rate which matches the magnetic anomalies interpretation of Burrus (1984). Equivalent half-spreading rates are 30 mm a^{-1} at a distance of 350 km and 6 mm a^{-1} at a distance of 70 km. Notice that since the pole of rotation is relatively

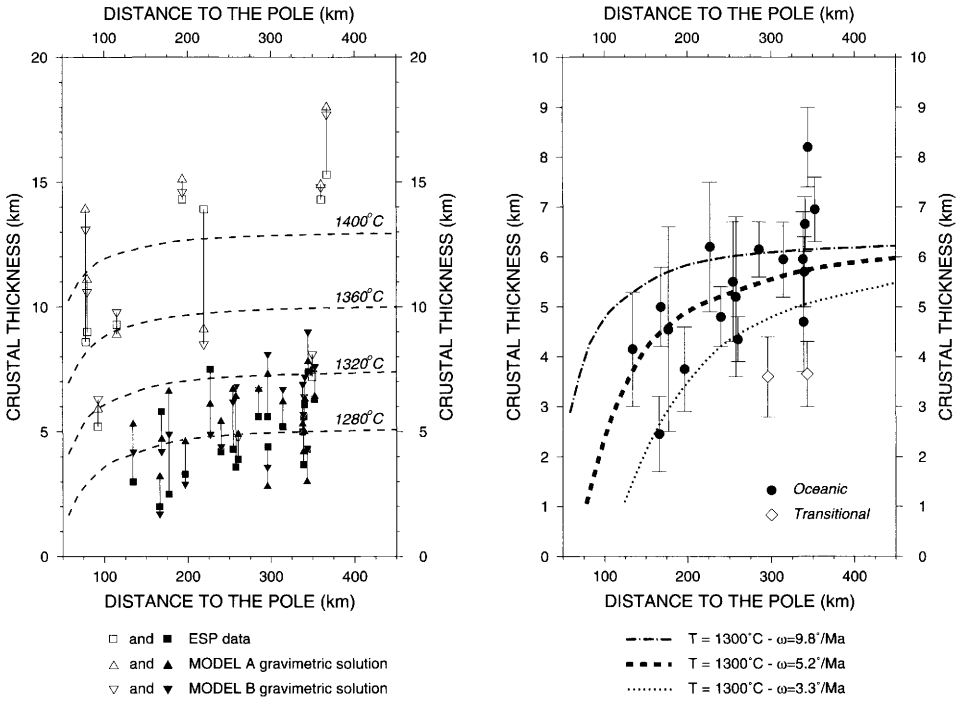

Fig. 9. (**a**) Crustal thickness (Model A, Model B and seismic refraction) at ESP points versus distance to the pole of opening. Dashed curves : predicted oceanic crustal thickness for various potential mantle temperature (1280–1400°C, from Bown & White 1994). A 30 mm a^{-1} half-spreading rate is assumed along the ECORS line (350 km away from the pole; spreading rate derived from Burrus 1984). Equivalent rotation rate is 9.8° Ma^{-1}. Filled symbols: oceanic or transitional type crust. Open symbols: continental crust. (**b**) Range of crustal thickness for oceanic crust (filled circles) and transitional type crust (open diamonds) versus distance to the pole of opening. Dashed curves are model predictions using the same mantle temperature (1300°C) but different rotation rates (9.8° Ma^{-1}, 5.2° Ma^{-1} and 3.3° Ma^{-1}, equivalent to 30 mm a^{-1}, 20 mm a^{-1} and 10 mm a^{-1} half-spreading rates along the ECORS line (section A, Fig. 4) and to 15 mm a^{-1}, 8 mm a^{-1} and 5 mm a^{-1} half-spreading rates in the Ligurian Sea (section E, Fig. 4).

close, spreading rate is directly proportional to the distance to the pole. A first-order interpretation of Fig. 9a is that all oceanic data points fall close to, or below, the predicted curve for a 1280°C potential temperature. This is about 30–50°C below normal temperature inferred at spreading centres away from hot spots and fracture zones (White *et al.* 1992; Bown & White 1994).

The same conclusion was reached independently from a 3D analysis of the subsidence in the Liguro-Provençal basin (Chamot-Rooke *et al.* in prep.). After corrections for sedimentary loading, for abnormal crustal thickness and for potential effects of the recent compression regime, subsidence is still about 500 m greater than expected from the age of the basin. A low potential mantle temperature would thus explain both the abnormal subsidence of the deep basin and the low magma supply during oceanic accretion, leading to the production of abnormally thin oceanic crust. Similar low-temperature boundary conditions may have also prevailed in the Tyrrhenian Basin (Réhault *et al.* 1990). This is not surprising since both the Liguro-Provençal Basin and the Tyrrhenian Basin opened as back-arc basins above the same lithospheric slab now subducting off Calabria (Le Pichon 1984; Malinverno & Ryan 1986). Thin crust and high subsidence have been reported in other marginal basins, in particular in the West Pacific. Low asthenospheric temperature may be the result of a long history of subduction of cold material, such as below the back-arc basins of the Philippine Sea plate for instance. In the Western Mediterranean, the amount of cold material subducted was probably much smaller, due to the slow convergence of

Africa towards Europe. Lithospheric thickening coeval with orogenic compression may also be an efficient way to lower temperatures at mantle depth, provided time span between compression and extension is short enough to prevent thermal equilibration. Extensional collapse of a former orogen is now well established for the origin of the Tyrrhenian Basin (Kastens *et al.* 1990; Jolivet *et al.* 1994). The potential role of the Pyrenean orogeny has also been discussed for the formation of Liguro-Provençal Basin (Mauffret *et al.* 1995), although the continuity of the Pyrenean belt towards the Gulf of Lion margin has not been clearly established so far.

A closer examination of Fig. 9a also shows the systematic trend observed along section G: oceanic crust becomes thinner closer to the pole of rotation, as predicted by melting models through spreading rate dependence. According to Bown & White (1994) models, a sharp decrease in melt production occurs at full spreading rates below 15 mm a^{-1}, whereas at higher rates the oceanic crust thickness is remarkably uniform (7 ± 1 km average, after White *et al.* 1992). Small oceanic crust thickness is well documented at the slow spreading Arctic ridge, where the crust is about 2.5 km thick for a 12–15 mm a^{-1} full rate (Jackson *et al.* 1982), and close to some of the Atlantic non-volcanic margins (review in Bown & White 1994; Srivastava & Roest 1995). In the Liguro-Provençal basin, a marked decrease in oceanic crust thickness occurs in the southernmost part of the Ligurian Sea, or 200 km away from the pole of rotation (Fig. 9a & b). The predicted full spreading rate there would be 34 mm a^{-1}, assuming a 9.8° Ma^{-1} rotation rate. This is more than twice the trade-off value of 15 mm a^{-1} inferred from modelling and observations.

The thin crust of the Ligurian Sea may result from two effects: (1) heat was lost laterally towards the adjacent continents (Provençal margin and Corsica), thus preventing large-scale melting even during oceanic accretion; (2) the rate of opening was half the value generally assumed, and consequently the critical 15 mm a^{-1} full spreading rate below which magma supply is small was reached at a distance of 200 km from the pole. The latter hypothesis is explored in Fig. 9b where we show the predicted oceanic crust thickness for different opening rates. A good solution is obtained if the opening rate is close to 5° Ma^{-1}.

Lateral heat conduction can be effective both during continental rifting and early oceanic spreading. During rifting, heat transfer from a hot extended area to cooler surroundings reduces significantly the amount of melt generated, so that even at potential temperature above normal, little or no melt is produced (Alvarez *et al.* 1984). This effect, combined with finite (as opposed to instantaneous) duration of rifting, explains the absence of significant amount of melt produced at non-volcanic continental margins (Bown & White 1995*a*, *b*). Lateral heat loss can also be efficient in reducing crustal thickness during the early phase of oceanic spreading. The time to establish a permanent thermal regime at the ridge axis is highly dependent on the spreading rate. At high spreading rates, the ridge will rapidly move away from the cooler adjacent continent. Conversely, small transient perturbations at slow spreading ridges will have large effects on the thickness of oceanic crust produced (Su *et al.* 1994). At high potential temperatures, the relative importance of buoyancy-driven mantle flow with respect to plate-driven mantle flow may even lead to an increase in crustal thickness with decreasing spreading rates (Su *et al.* 1994). However, at low to normal potential temperatures as those considered here, plate-driven flow will dominate and variations in crustal thickness will basically reflect variations in the temperature field. How far the ridge temperature field is affected by the proximity of the continent depends not only on the oceanic spreading rate but also on the kinematics of stretching. For short rifting duration and high thinning factor, reducing the continental crust to oceanic crust thickness, the stretched continental crust is thermally indistinguishable from oceanic crust. More generally, the duration of rifting and the amount and distribution of thinning, as well as spreading rate, will control the temperature field and thus oceanic crust genesis at the ocean–continent boundary.

A convenient way to estimate the time needed to establish a steady-state thermal regime at the ridge axis is to follow the abnormal subsidence induced by lateral conduction towards cooler continent. Section E, located in Fig. 4, crosses the area of abnormally thin oceanic crust at the southernmost end of the Ligurian Sea. A thermal model including continental rifting (from 30 to 23 Ma), oceanic spreading (from 23 to 19 Ma) and post-spreading cooling (from 19 Ma to present) was already presented and discussed in a previous section (see Fig. 7). We are interested now in the very early phase of oceanic spreading. The rifting history and amount of stretching is taken identical to the model of Fig. 7. The steady-state solutions (including lateral conduction) for intermediate (40 mm a^{-1}) and slow (18.5 mm a^{-1}) spreading are shown as large dots in Fig. 10. This is equivalent to the ocean-continent boundary being located at an infinite distance from the

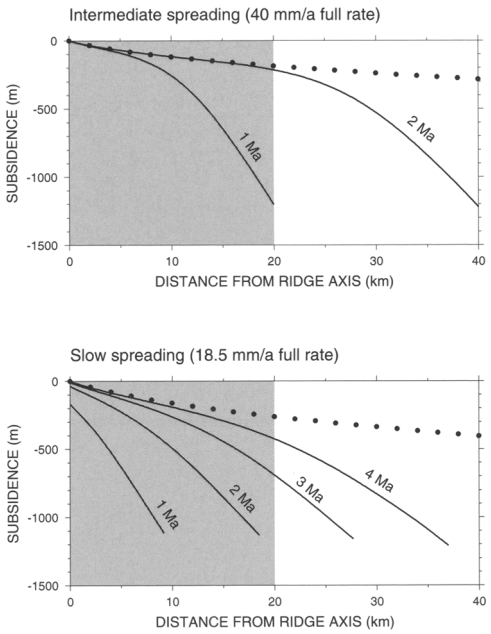

Fig. 10. (**a**) Predicted subsidence of the oceanic lithosphere as a function of proximity of the ocean-continent boundary. An intermediate full spreading rate of 40 mm a^{-1} is assumed. The ridge axis remains located on the left of the diagram, whereas the ocean–continent boundary (OCB) is progressively moving away. The 2D steady-state solution (ocean–continent boundary at infinity) is shown by large dots. Thin lines are subsidence curves (below water) from the ridge axis to the OCB, 1 Ma (OCB at 20 km) and 2 Ma (OCB at 40 km) after initiation of spreading (modelled section is section E in Fig. 4). The shaded grey area is the location of maximum melt extraction. (**b**) Same as (**a**) for slow spreading (18.5 mm a^{-1} full rate, equivalent to best value obtained from Fig. 9b).

ridge axis. We then model the transient regime as the ocean–continent boundary moves away from the ridge axis. At high spreading rate, the steady-state regime at the ridge axis is reached in less than 1 Ma (in other words, the proximity of the continent no longer affect the ridge thermal regime). In the slow spreading case, thermal equilibrium at the ridge axis is reached within 3 Ma. Even though melt production rates decrease rapidly with distance from the ridge, melt extraction may not be limited to the ridge axis itself. The lateral dimension of the melting region is still a matter of debate (e.g. Scott & Stevenson 1989; Cordery & Morgan 1993). It may reach several tens of kilometres, in which case the melt would be focused towards the ridge axis (Spiegelman & McKenzie 1987). In terms of volume, however, melting models seem to indicate that about 80–90% of the melt that will contribute to oceanic crust genesis is produced within 20–30 km of the ridge axis. For the Ligurian Sea section, a steady-state regime over such distances will be reached within 2 Ma at a high spreading rate (40 mm a^{-1}); at a lower spreading rate (18.5 mm a^{-1}), it may take more than 4 Ma to establish a permanent thermal regime (see Fig. 10). The total oceanic basin width would then be 80–100 km in both cases. Above this width, lateral conduction towards continent no longer affects the temperature field in the area where melt extraction is maximum. Notice that we discuss here the area where melt extraction is maximum, and not the total width of the melting region which may reach 80 to 100 km (Cordery & Morgan 1993).

The width of the oceanic domain along the modelled Ligurian Sea section is between 60 and 80 km. A first conclusion is that lateral conduction cannot be neglected, in particular if spreading was slow. Part of the anomalous oceanic crustal thickness may be the result of side heat loss towards both continental masses (Provence and Corsica). Northward, lateral cooling during rifting may even have been sufficiently large to prevent large-scale melting and the formation of oceanic crust. For similar stretching factors and duration of rifting, the critical total basin width may be of the order of 70–100 km (Alvarez *et al.* 1984), which is about the size of the northernmost Ligurian Sea basin. Notice that along section F, crustal thickness is clearly too thick to be compatible with an oceanic origin (Fig. 8). Three coeval effects will act to lower considerably magma supply: (1) a low spreading rate due to the proximity of the pole of opening; (2) a low potential temperature, as discussed previously; (3) high lateral conduction due to the small basin width. Oceanic crust produced, if any, would necessary be very thin. The northernmost Ligurian Sea is thus most probably floored with thinned continental crust.

An important implication of our thermal modelling is that thin abnormal oceanic crust, formed during the early stage of oceanic spreading, can be found within 40–50 km of the ocean–continent boundary. Variability of oceanic crust thickness is thus expected to be found not only along strike, as an effect of a narrowing basin towards the Ligurian Sea, but also across strike, close to the ocean–continent boundary. In the following sections, we first discuss estimates of the opening rate of the Liguro-Provençal Basin, since it is one of the important parameters controlling melting and oceanic crust genesis. We then examine the early

oceanic stage leading to the formation of oceanic crust close to the ocean-continent boundary.

Rate and timing of the Corsica–Sardinia block rotation

Estimates of the rate and timing of opening of the Liguro-Provençal basin have been obtained from different types of data: structural restoration of the position of the Sardinia–Corsica block, based on pre-rotation markers (e.g. Westphal *et al.* 1976), seismic stratigraphy of pre-rift, syn-rift and post-rift horizons (e.g. Mauffret *et al.* 1995), age of volcanism in Sardinia (Bellon *et al.* 1977), palaeomagnetic data in Sardinia (Montigny *et al.* 1981) and Corsica (Vigliotti & Kent 1990), identification of the magnetic anomalies in the oceanic domain (Burrus 1984), age of dredged samples in the basin (Réhault 1981). We focus here on evidence for age and rate of oceanic spreading leading to quantitative estimates: age of dredged samples, age of magnetic lineations, age and amount of rotation of Sardinia and Corsica rocks derived from palaeomagnetism.

The basement is buried below a thick sedimentary cover over the entire Liguro-Provençal basin, with the exception of an exposed ridge in the Ligurian Sea. The southernmost part of the Ligurian Sea is floored with very thin oceanic crust. Crustal thickness gradually increases towards the northeasternmost portion of the Ligurian Sea, which is most probably floored with stretched continental crust (see previous section). Along section F (Fig. 8) the crust is thin at ESP 224 only (5–6 km). Immediately east of it (ESP 223) runs an axial N30°-trending linear ridge cropping out at its northernmost end (Réhault 1981; Réhault *et al.* 1984). The ridge was sampled by dredging, and tristanite samples of mid-Miocene age were recovered (18 ± 0.5 Ma in Réhault *et al.* 1984). Recent re-dating would indicate a younger 17 Ma age (Réhault pers. comm. 1996). The tristanite ridge coincides with the central magnetic anomaly high recognized throughout the basin and may thus represent the latest magmatic rocks erupted at the end of the spreading phase (Réhault *et al.* 1984). The discrepancy between the age of anomaly 6, proposed as the axial anomaly (Burrus 1984), and the age of the tristanite ridge has already been mentioned in Réhault *et al.* (1984). Anomaly 6 normal polarity interval lasted 1 Ma, from *c.* 20.3 to 19.3 Ma (Berggren *et al.* 1985; Harland *et al.* 1990). A 17 Ma age would be more compatible with anomaly 5C (three triplets closely spaced in time between 16.2 and 17 Ma) rather than anomaly 6. The alternative is that the tristanite ridge erupted after cessation of spreading. Then the positive magnetic anomaly of the ridge, aligned with the positive axial anomaly of the basin, would be fortuitous.

Additional constraints are given by the timing of the rotation of the Sardinia–Corsica block. The amount of Tertiary rotation has been widely debated. Apart from structural evidences based on a common geological history of the Sardinia–Corsica block and the Provençal mainland (e.g. Westphal *et al.* 1976), palaeomagnetic measurements allowed various determinations of the amount and timing of the rotation. Data used range from palaeomagnetic measurements on the Tertiary volcanic rocks of Sardinia (Bellon *et al.* 1977; Edel & Lörtscher 1977; Edel 1979; Montigny *et al.* 1981), aeromagnetic measurements over Sardinia (Galdéano & Ciminale 1987), and finally palaeomagnetic study of the Tertiary sediments from Corsica (Vigliotti & Kent 1990), since Tertiary calc-alkaline volcanism is absent there. Different data sets consistently point to a 30–40° counterclockwise rotation of the Sardinia–Corsica block with respect to stable Europe. The timing of the rotation, however, remains uncertain. Dating relies both on K–Ar age determinations of the Sardinia andesitic and ignimbritic suite, compiled in Montigny *et al.* (1981), and Miocene fossiliferous limestones of the Neogene basins of Corsica (Vigliotti & Kent 1990). Both sets of data are apparently conflicting. Montigny *et al.* argue for a 20.5–19 Ma (early Burdigalian) rapid rotation. This is the solution retained by Burrus (1984) to identify magnetic lineations previously delineated by Bayer *et al.* (1973). Vigliotti & Kent, on the other hand, conclude that a rotation of about 20° was still to be completed in post-Burdigalian–Langhian time. They propose that the rotation did not end before 15 Ma (late Langhian). Their results are controversial not only because they contradict the Montigny *et al.* compilation, but also, as they state themselves, because secondary magnetization cannot be completely ruled out. However, their conclusion is not different from that initially reached by Bellon *et al.* (1977) from their palaeomagnetic study of the Tertiary volcanism of Sardinia.

Palaeomagnetic data from the Montigny *et al.* compilation for Sardinia and the Vigliotti & Kent data for Corsica are summarized in Fig. 11. Notice that we use all data reported in Montigny *et al.* rather than a selection of the data set. Youngest ages, in particular, were systematically omitted in their original plot. Results obtained from the sedimentary rocks of Corsica by

Vigliotti & Kent are actually not incompatible with Sardinian palaeomagnetic measurements (see also Vigliotti & Langenheim 1995). Although scattering for the Sardinia volcanic rocks is high, it is clear that all rocks, regardless of their ages, show a westward oriented magnetization. Taking into account the apparent polar wander path for Eurasia, the Miocene pole position predicts a +7° palaeomagnetic declination at the location of the Sardinia–Corsica block (Vigliotti & Kent 1990). The conclusion is that almost none of the observed sites, in the range 35–15 Ma, remained stable with respect to Eurasia. Although a rapid rotation cannot be completely ruled out, a much slower rotation ending in Langhian or Serravalian time would still be compatible with the palaeomagnetic data.

Magnetic anomalies interpretation in the oceanic domain is rather inconclusive. The well-lineated axial positive anomaly is bounded by one additional positive anomaly on both sides, so that only three anomalies are available for age identification. Considering the set of possible anomalies in the range 25–10 Ma, most of which are more or less regularly spaced in time every 1 Ma, several interpretations are possible. The recognition of the axial anomaly as anomaly 6 (20 Ma) is clearly not compatible with available palaeomagnetic data. If the identification of the Late Burdigalian horizon throughout the basin is correct (Mauffret *et al.* 1995), then the oceanic crust cannot be younger than 16 Ma. Further, onlapping of this horizon on the basement in the axial part of the basin would still have to be proved. Could this horizon be younger, and the Late Burdigalian be deeper? A possible deeper candidate for the Late Burdigalian horizon is present on the ECORS seismic line (horizon X in de Voogd *et al.* 1981). This horizon is onlapping the acoustic basement a few tens of kilometres away from the inferred location of the fossil ridge. Stratigraphic correlation of the Late Burdigalian from GLP2 well

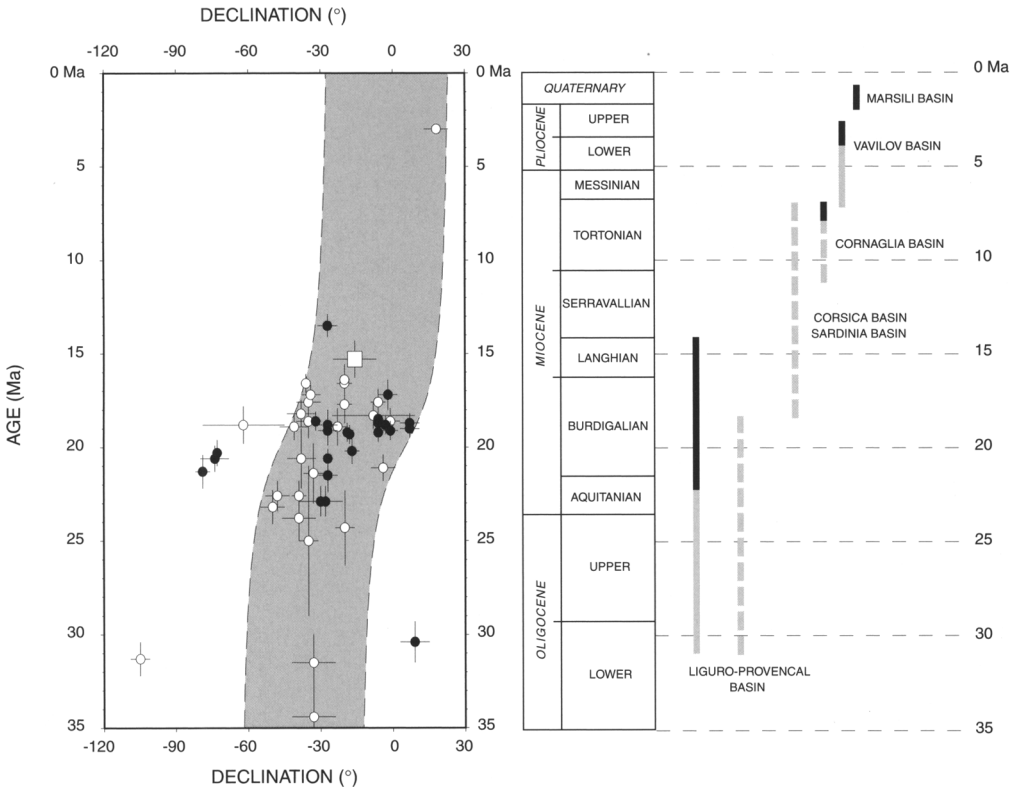

Fig. 11. Palaeomagnetic data for the Tertiary volcanic rocks of Sardinia (after Montigny *et al.* 1981; filled dots, normally magnetized; open dots, reversely magnetized) and for the Miocene sedimentary rocks of Corsica (square symbol; after Vigliotti & Kent 1990). The timing of Western Mediterranean basins opening is shown on the right (dark line, oceanic spreading; grey lines, continental rifting, dashed if not well constrained).

(close to ESP 202 on the upper Gulf of Lion margin) to the deep basin would then have to be reconsidered.

The exact age of oceanic spreading in the Liguro-Provençal basin is thus still open to discussion. Cessation of spreading in Late Burdigalian time (16.5 Ma) would be more or less compatible with palaeomagnetism, stratigraphic correlations and age of the tristanite ridge. Palaeomagnetism alone would tend to indicate an even younger Langhian age (14 Ma?). Calc-alkaline volcanic rocks erupted in Sardinia until 13 Ma (Bellon *et al.* 1977), indicating that subduction was still going on beneath, and that the source for volcanism moved away not before that time (possibly in relation to opening of the Tyrrhenian Basin). Notice that the heat flow in the axial part of the basin is well above 120 mW m^{-2}, which is the theoretical value for a 15 Ma aged basin. Even in the more conservative hypothesis, oceanic spreading between 23 Ma (post-syn-rift Early Aquitanian deposits) and 16.5 Ma (pre-Late Burdigalian) requires reconsideration of spreading rate estimates. The width of the oceanic domain along the ECORS line (section A, Fig. 8) is between 150 km (Mauffret *et al.* 1995) and 230 km (Burrus 1984 or Réhault *et al.* 1984). Since no differential rotation was found in the palaeomagnetic data between 30 and 23 Ma, most of the rotation was thus achieved during the oceanic spreading phase (Bellon *et al.* 1977; Burrus 1984). A small oceanic domain, less than 200 km wide, can then be excluded. This would locate the pole of rotation too close (somewhere in the southern Ligurian Sea) to reach the 40° rotation of the Corsica–Sardinia block. A self-consistent solution is obtained if the oceanic width is 230 ± 20 km. The pole of rotation is found 330 km away, somewhere in the Gulf of Genoa, close to the location discussed previously. The mean full spreading rate would then be 30 ± 5 mm a^{-1}, about half the value assumed in Burrus (1984).

Plate separation rates during rifting can be estimated from the amount of stretching across extended conjugate margins. Assuming that the volume of continental crustal rocks remained constant during rifting, calculations for section A (Fig. 12) indicate about 150 ± 30 km of total continental extension (i.e. displacement of Sardinia; similar estimates are found in Le Douaran *et al.* 1984). Taking into account the duration of rifting (7–10 Ma), the mean plate separation rate during rifting was then 20 ± 7 mm a^{-1}, to be compared to 30 ± 5 mm a^{-1} during spreading. We thus favour a continuous extension mechanism throughout the basin history, rather than a sudden pulse of oceanic accretion. Extension in the Liguro-Provençal basin was then relieved by the opening of the Tyrrhenian basin. Although rifting in the Tyrrhenian basin may have started as early as Early Miocene (post-early-Burdigalian?, Sartori 1990), the entire basin was not rifted until Tortonian (9 Ma, Sartori 1990; Kastens *et al.* 1990). Extension was, however, already active in Alpine Corsica in Late Oligocene or Early Miocene time, since ductile extension there ended with the deposition of well-dated Burdigalian limestones in Corsica and Langhian sediments in the Corsica Basin (Jolivet *et al.* 1991, 1994). During Pliocene time, oceanic crust was produced in two small oceanic basins (Kastens *et al.* 1990), the Vavilov basin (possibly spreading in Early Pliocene time) and Marsili basin (younger than 2 Ma). The recent Médée survey revealed that the toe of the Calabrian prism in the Ionian Sea is no longer active (Le Pichon *et al.* pers. comm.), indicating that extension in the Tyrrhenian Sea may have recently ceased (notice that post-spreading volcanism may be active with little or no extension, as found in many of the back-arc basins of the West Pacific).

Drilling results in the Tyrrhenian Sea (Kastens *et al.* 1990) are compatible with the outward arc migration model of Malinverno & Ryan (1986) which emphasizes the role of 'rollback' (slab retreat) of the African subduction hinge zone, now located in the Ionian Sea. Restoration of the Tyrrhenian margins to their original widths is somewhat speculative, in particular for the north Calabrian margin. According to Malinverno & Ryan (1986), the total extension (continental stretching plus oceanic spreading) across the basin was 330–350 km, uncertainty amounting to several tens of kilometres. Notice that this is close to the amount of extension obtained on Section A across the Gulf of Lion and Sardinia margin (380 ± 50 km), thus suggesting some sort of self-regulating mechanism (such as distance from the subduction front to the back-arc accreting ridge). If we assume that rifting in the Tyrrhenian began 9 Ma ago, then the mean opening rate would be 40 mm a^{-1}. This may be regarded as a maximum value. If we include significant pre-Tortonian rifting, the opening rate may be as low as 20 mm a^{-1} (Malinverno & Ryan 1986). A high oceanic spreading rate was reported in the Marsili basin (70–80 km over a 2 Ma period, 40 ± 5 mm a^{-1}, Kastens *et al.* 1990), but the exact width of the oceanic domain remains uncertain.

The total extension in the Liguro-Provençal and Tyrrhenian basins, taken along a N135° azimuth, is thus of the order of 700 km (±100 km) since Oligocene time. Opening most

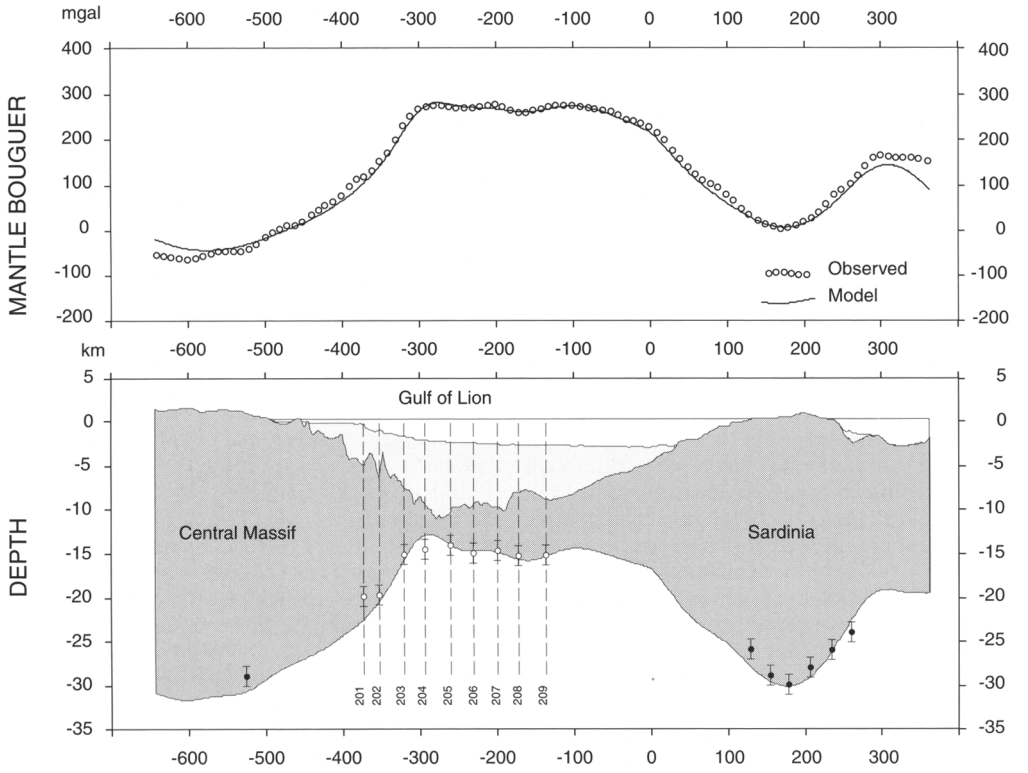

Fig. 12. Crustal section obtained from 3D gravity inversion (Model A solution) along the ECORS profile (section A located in Fig. 4; Fig. 8 top). Top: observed and modelled Bouguer.

probably became effective once the entire Liguro-Provençal basin was rifted (possibly in Late Oligocene time). Le Pichon (1984) compared this amount of extension with the present-day length of the Calabrian seismic zone. The seismic slab is 650 km long, dipping 70° along a N315° azimuth (Selvaggi & Chiarabba 1995). Convergence of Africa towards Europe since the Burdigalian may be more than 200 km in that part of the Mediterranean Sea (Dewey *et al.* 1989), or 150 km taken along the azimuth of the slab. The remaining 500 km can thus be directly compared to the amount of extension in the Western Mediterranean basins. The length of the slab is clearly too long compared to the amount of extension in the Tyrrhenian basin only. If the Liguro-Provençal basin is included, then total extension becomes greater than the length of the seismic slab. Le Pichon (1984) concluded that part of the slab (the last 200 km, subducted in Late Oligocene time) may now be aseismic following reheating at depth. This may be substantiated by tomographic results (e.g. De Jonge *et al.* 1994), but resolution becomes poor below 400 km depth.

The succession of basins opening thus suggests a continuum of extension since Oligocene time, with progressive southeastward migration of basins formation following rollback of the African hinge zone as proposed by Malinverno & Ryan (1986). We suggest that the time gap between opening of the Liguro-Provençal Basin and stretching of the Tyrrhenian Basin should be reconsidered. Cessation of spreading in the Liguro-Provençal basin 19 Ma ago (as generally assumed), and post-Tortonian rifting of the Tyrrhenian Basin (post-10 Ma) would imply high velocity African trench retreat in the early stage (> 60 mm a^{-1}), followed by strike-slip motion for 10 Ma (to accommodate the northward motion of Africa with respect to the Corsica–Sardinia–Calabria block then belonging to Europe), and finally subduction again (> 40 mm a^{-1}) during Tyrrhenian opening. We favour a model in which trench retreat proceeded at a more or less constant velocity

(30–40 mm a^{-1}) while consuming the old Ionian oceanic lithosphere. Side continental collisions (in the Northern Apennines, between the Kabylies and Africa, in Sicily) may have slowed down the upper plate motion locally, without affecting significantly subduction motion along the remaining oceanic portions of the Ionian lithosphere driven by slab pull (Le Pichon 1982; Le Pichon & Alvarez 1984).

Crust at the ocean–continent boundary

The western portion of section A (Figs 7 and 8) is along the ECORS deep-seismic profile and cut across ESP 201 to 209 mid-points. Eastern portion of section B is close to the CROP deep-seismic line. The two sections illustrate the contrast between the wide and smoothly stretched Gulf of Lion margin and the narrow and abruptly stretched Provençal margin. On both sections a very thin crust (2–3 km) is found at the base of the lower continental margin (ESP 204 on section A, ESP 211 on section B). Our gravity modelling suggests that thin crust should also be found over the conjugate Sardinian margin (Fig. 4), but no further seismic information is available there.

On the Gulf of Lion margin, the detailed analysis of Pascal *et al.* (1993), based on x-t to τ-p transformations and synthetic τ-p seismograms, provides reliable P-wave velocity structure down to Moho depth. The upper crust over the entire basin, including thin continental and oceanic domains, is characterized by a 5.6–5.8 km s^{-1} velocity layer. The mid-crust velocity increases laterally oceanward from ESP 203 and 212 to ESP 204 and 211 respectively, from 6.2 to 6.6 km s^{-1}. Below the thin crust area is a high-velocity layer with velocities ranging from 7.1 to 7.4 km s^{-1}. The thickness of the high-velocity layer is maximum at ESP 203 (2.6 km) and at ESP 212 (2.9 km). It reaches 1 km at ESP 211 and 212. As pointed out by Mauffret *et al.* (1995), the high-velocity layer is apparently not restricted to the very base of the margin, but extends oceanward (0.4 km thick at ESP 205 and 1.4 km thick at ESP 206). At the base of the Gulf of Lion margin, the top of the high P-wave velocity body correlates with the oceanward rising of a shallow bright reflector on the ECORS line ('T' reflector in Pascal *et al.* 1993). The T reflector comes very close to the top of basement between ESP 211 and 212 (LIGO 4 seismic profile, Pascal *et al.* 1993). This is also the area of thinnest crust in our gravity inversion. Landward, the T reflector coincides with Moho.

The continent–ocean boundary has been placed at various locations along the ECORS line: close to ESP 203 based on magnetic anomalies (Bayer *et al.* 1973), between ESP 205 and ESP 206 based on the limit of synrift deposits (Burrus 1984; Le Douaran *et al.* 1984), and more recently as far as ESP 206 based mainly on the lack of the high velocity layer beyond this point (Mauffret *et al.* 1995), typical oceanic layer 3 velocities (6.8 km s^{-1}) being found at ESP 207. In the latter case, the transitional area (possibly thinned continental crust) would be 100 km wide.

Thin crust at the base of the Gulf of Lion shows strong similarities with transitional type crust observed on other non-volcanic margins. Thin crust overlying a high velocity layer is found on the western margin of Iberia (3–4 km thick above a 7.3–7.6 km s^{-1} layer, Whitmarsh *et al.* 1990, 1993), in the Tagus abyssal Plain (2 km thick above 7.6 km s^{-1} layer increasing to 7.9 km s^{-1} towards Moho, Pinheiro *et al.* 1992) and its conjugate Newfoundland margin off Grand Banks (2–3 km thick above a 7.2–7.7 km s^{-1} layer, Reid 1994), across Southwest Greenland margin (2.5 km thick above 7.0–7.6 km s^{-1} layer, Chian & Louden 1994) and its conjugate Labrador margin (1–2 km thick above a 6.4–7.7 km s^{-1} layer, Chian *et al.* 1995). On the southern Newfoundland margin the high-velocity body is limited by one or two landward-dipping reflectors rising to basement surface seaward and connecting to Moho landward (Keen & de Voogd 1988; Reid 1994). The similarity with the T reflector of the Gulf of Lion is striking.

The origin of the high velocity lower crust on non-volcanic margins (underplating or serpentinite ?) and the nature of the thin overlying crust is still debated (Chian *et al.* 1995; Srivastava & Roest 1995). Further discussion is beyond the scope of this paper, although much could be learned by integrating the Gulf of Lion data into a much broader review of tectonic processes at non-volcanic margins. A few conclusions can, however, be drawn from the preceding sections. Underplating is very unlikely. Taking into account cooling during rifting (which lasted at least 7 Ma) and low initial mantle temperature (30–50°C below normal), the amount of melt generated during rifting was probably very small as for other non-volcanic margins (Bown & White 1995*a*). The thin crust flooring the lower margin of the Gulf of Lion as well as the lower margin of Sardinia may be of oceanic origin. Thermal modelling (Fig. 10) demonstrates that the width of abnormal thin oceanic crust may reach 40–50 km, which is about the right amount obtained by gravimetric

modelling and seismic refraction (see sections in Fig. 8).

Conclusions

The deep structure of the Liguro-Provençal Basin is discussed using gravity as an additional control to existing sparse seismic data. The main results can be summarized as follows.

(1) 3D gravity inversion using Fourier transforms is a potential powerful tool to obtain a reliable geometry of the Moho discontinuity in areas where only sparse deep seismic informations are available. Free parameters in the inversion (Moho reference depth and crust-mantle density contrast) can be obtained through least squares minimization of the standard deviation of the gravimetric solution at some given reference points where the Moho is seismically constrained, such as ESP data. The misfit in the Liguro-Provençal Basin is about 2 km for a 12–30 km Moho depth range. Corrections for variable crust density and variable heat flow distribution can also be included, although in the particular case of the Liguro-Provençal Basin they do not improve significantly the solution.

(2) The oceanic crust thickness in the Liguro-Provençal Basin is smaller than usually reported in open oceans (5 ± 1 km instead of 7 ± 1 km). We show that the thin oceanic crust is compatible with a 1280°C potential mantle temperature, which is 30–50°C below normal. Low temperature is also responsible for the abnormal subsidence of the deep Liguro-Provençal Basin. Thin crust and high subsidence have been reported in other marginal basins, in particular in the West Pacific. Subduction of cold material may be responsible for significant cooling at depth. However, thermal conduction is slow and would probably require a long history of subduction. For the same reason (slow conductive process), lithospheric thickening coeval with orogen formation and prior to extension may be a more efficient way to lower temperatures at mantle depth.

(3) The decrease of oceanic crust thickness towards the Ligurian Sea to values as small as 2 km indicates a very low magma supply. The temperature field there is affected by two different effects, both of conductive origin : heat is lost laterally towards the adjacent continents (Provençal margin and Corsica), thus preventing large-scale melting even during oceanic accretion; rate of opening in the Ligurian Sea falls below the critical 15 mm a^{-1} full spreading rate below which magma supply becomes negligible. An important implication is that in the northern Ligurian Sea, where lateral conduction is maximum and distance to the pole of opening minimum, the crustal thickness is too thick to be of oceanic origin.

(4) The thin crust at the ocean–continent boundary may be oceanic crust produced in the very early stage of oceanic spreading, as proposed for some of the non-volcanic Atlantic margins. Several million years are required to establish a steady-state thermal regime at the ridge axis, due to lateral cooling towards unextended continental areas. The lower margin of the Gulf of Lion has actually many of the characteristics encountered on other non-volcanic margins: tilted blocks rooted on a seaward-dipping reflector, high P-velocity body bounded to the top by a landward-dipping reflector, and connecting at depth with Moho towards the continent, very thin crust in the transitional region from thinned crust to oceanic crust.

(5) A close re-examination of magnetic data (palaeomagnetic data and magnetic lineations) shows that the exact age of oceanic spreading, as well as the opening rate, is still debatable. Cessation of spreading in Late Burdigalian time (16.5 Ma) would be a reasonable compromise between somewhat divergent palaeomagnetism, stratigraphic interpretation and age of dredged samples data. An even younger age cannot be completely ruled out. In any case, we favour a constant and slow opening at a rate of 5° Ma^{-1}, rather than a sudden pulse of oceanic accretion.

(6) The new Moho depth map is used to estimate the amount of extension across the Liguro-Provençal Basin. Comparison with the Tyrrhenian Basin and length of the Calabrian slab suggests a continuous extension mechanism since Oligocene time driven by the African trench retreat, following Malinverno & Ryan (1986) model. It is suggested that the process continued uninterrupted until recent time, unless drastic velocity changes occurred at the subduction zone where the old Ionian oceanic lithosphere was being consumed.

This paper is within the framework of the Integrated Basin Studies (IBS) program. We are grateful to G. Pascal for his helpful comments on reflection and refraction data interpretation. Stimulating lectures given by X. Le Pichon at Collège de France in 1996 helped in clarifying some of the ideas developed here. We thank our colleagues who made available to us some of their unpublished data, in particular A. Mauffret for his digital file of sediment thickness around the Gulf of Lion margin and C. Truffert for some new processed maps of the magnetic field.

References

ALVAREZ, F., VIRIEUX, J. & LE PICHON, X. 1984. Thermal consequences of lithosphere extension

over continental margins : the initial stretching phase. *Geophysical Journal of the Royal Astronomical Society*, **78**, 389–411.

ANGUY, Y., DAMOTTE, B. & ROURE, F. 1991. Tirs sismiques latéraux complémentaires au profil ECORS-Pyrénées : apport à la connaissance de l'architecture profonde de la chaîne. *Comptes rendus de l'Académie des Sciences, Paris, sér. D*, **313**, 677–684.

ARTHAUD, F., OGIER, M. & SÉGURET, M. 1980. Géologie et Géophysique du golfe du Lion et de sa bordure nord. *Bulletin du Bureau de Recherches géologiques et minières*, **1**, 175–193.

BANDA, E., ANSORGE, J., BOLOIX, M. & CORDOBA, D. 1980. Structure of the crust and upper mantle beneath the Balearic islands (western Mediterranean). *Earth and Planetary Science Letters*, **49**, 219–230.

BAYER, R., LE MOUEL, J.-L. & LE PICHON, X. 1973. Magnetic anomaly pattern in the Western Mediterranean. *Earth and Planetary Science Letters*, **19**, 168–176.

BELLON, H., COULON, C. & EDEL, J.-B. 1977. Le déplacement de la Sardaigne. Synthèse des données géochronologiques, magmatiques et paléomagnétiques. *Bulletin de la Société géologique de France*, **7**, 825–831.

BERGGREN, W. A., KENT, D. V., FLYNN, J. J. & VAN COUVERING, J. A. 1985. Cenozoic geochronology. *Geological Society of America Bulletin*, **96**, 1407–1418.

BESSIS, F. 1986. Some remarks on the study of subsidence of sedimentary basins. Application to the Gulf of Lions margin (Western Mediterranean). *Marine and Petroleum Geology*, **3**, 37–63.

BOWN, J. W. & WHITE, R. S. 1994. Variation with spreading rate of oceanic crustal thickness and geochemistry. *Earth and Planetary Science Letters*, **121**, 435–449.

—— & —— 1995*a*. Effect of finite extension rate on melt generation at rifted continental margins. *Journal of Geophysical Research*, **100**, 18011–18029.

—— & —— 1995*b*. Finite duration rifting, melting and subsidence at continental margins. *In*: BANDA, E., TORNÉ, M. & TALWANI, M. (eds) *Rifted Continent–Ocean Boundaries*. Kluwer Academic Press, Netherlands, 31–54.

BURRUS, J. 1984. Contribution to a geodynamic synthesis of the Provençal Basin (North-Western Mediterranean). *Marine Geology*, **55**, 247–269.

—— 1989. Review of geodynamic models for extensional basins; The paradox of stretching in the gulf of Lions (Northwest Mediterranean). *Bulletin de la Société géologique de France*, **8**, 377–393.

CHEN, Y. J. 1992. Oceanic crustal thickness versus spreading rate. *Geophysical Research Letters*, **19**, 753–756.

CHIAN, D. & LOUDEN, K. E. 1994. The continent-ocean crustal transition across the southwest Greenland margin. *Journal of Geophysical Research*, **99**, 9117–9136.

——, —— & REID, I. 1995. Crustal structure of the Labrador Sea conjugate margin and implications for the formation of non-volcanic continental margins. *Journal of Geophysical Research*, **100**, 24239–24253.

CHOUKROUNE, P. & TEAM, E. 1989. The ECORS pyrenean deep seismic profile reflection data and the overall structure of an orogenic belt. *Tectonics*, **8**, 23–39.

——, ROURE, F., PINET, B. & TEAM, E. P. 1990. Main results of the ECORS Pyrenees profile. *Tectonophysics*, **173**, 411–423.

CORDERY, M. J. & MORGAN, J. P. 1993. Convection and melting at mid-ocean ridges. *Journal of Geophysical Research*, **98**, 19477–19503.

COWIE, P. A. & KARNER, G. D. 1990. Gravity effect of sediment compaction : examples from the North Sea and the Rhine Graben. *Earth and Planetary Science Letters*, **99**, 141–153.

DANOBEITIA, J. J., ARGUEDAS, M., GALLART, J., BANDA E. & MAKRIS, J. 1992. Deep crustal configuration of the Valencia trough and its Iberian and Balearic borders from extensive refraction and wide-angle reflection seismic profiling. *Tectonophysics*, **302**, 37–55.

DE JONGE, M. R., WORTEL, M. J. R. & SPAKMAN, W. 1994. Regional scale tectonic evolution of the seismic velocity structure of the lithosphere and the upper mantle: the Mediterranean region. *Journal of Geophysical Research*, **89**, 12091–12108.

DE VOOGD, B., NICOLICH, R., & 21 OTHERS. 1991. First deep seismic reflection transect from the Gulf of Lions to Sardinia (Ecors-Crop profiles in Western Mediterranean). *In: Continental lithosphere: deep-seismic reflections*. American Geophysical Union, 265–274.

DELLA VEDOVA, B., LUCAZEAU, F., PASQUALE, V., PELLIS, G. & VERDOYA, M. 1995. Heat flow in the tectonic provinces crossed by the southern segment of the European Geotraverse. *Tectonophysics*, **244**, 57–74.

DEWEY, J. F., HELMAN, M. L., TURCO, E., HUTTON, D. H. W. & KNOTT, S. D. 1989. Kinematics of the western Mediterranean. *In*: COWARD, M.P., DIETRICH, D. & PARK, R.G. (eds) *Alpine Tectonics*. Geological Society, London, Special Publications, **45**, 265–283.

EDEL, J.-B. 1979. Paleomagnetic study of the Tertiary volcanics of Sardinia. *Journal of Geophysics*, **45**, 259–280.

—— & LÖRTSCHER, A. 1977. Paléomagnétisme du volcanisme tertiaire de Sardaigne. Nouveaux résultats et synthèse. *Bulletin de la Société géologique de France*, **7**, 815–824.

EGGER, A. 1992. *Lithospheric structure along a transect from the northern Apennines to Tunisia derived from seismic refraction data*. PhD Thesis, Swiss Federal Institute of Technology, Zürich.

——, DEMARTIN, M., ANSORGE, J., BANDA, E. & MAIESTRELLO, M. 1988. The gross structure of the crust under Corsica and Sardinia. *Tectonophysics*, **150**, 363–389.

FOUCHER, J. P., LE PICHON, X. & SIBUET, J. C. 1982. The ocean–continent transition in the uniform lithospheric stretching model; role of partial melting in the mantle. *In*: KENT, P., BOTT, M. H. P.,

McKENZIE, D. P. & WILLIAMS, C. A. (eds) *Evolution of sedimentary basins. Philosophical Transactions of the Royal Society of London*, **A305**, 27–43.

GALDÉANO, A. & CIMINALE, M. 1987. Aeromagnetic evidence for the rotation of Sardinia (Mediterranean Sea): comparison with the paleomagnetic measurements. *Earth and Planetary Science Letters*, **82**, 193–205.

GALLART, J., DAIGNIÈRES, M., BANDA, E., SURINACH, E. & HIRN, A. 1980. The eastern Pyrenean domain: lateral variations at crust-mantle level. *Annales Geophysicae*, **36**, 2, 141–158.

GIESE, P., MORELLI, C. & STEINMETZ, L. 1973. Main features of crustal structure in western and southern Europe based on data of explosion seismology. *Tectonophysics*, **20**, 367–379.

GORINI, C. 1993. *Géodynamique d'une marge passive: le Golfe du Lion (Méditerranée Occidentale)*. Thèse de 3ème cycle, Toulouse.

HARLAND, W. B., ARMSTRONG, R. L., COX, A. V., CRAIG, L., SMITH, A. G. & SMITH, D. G. 1990. *A geologic time-scale 1989*. Cambridge University Press, New York.

JACKSON, H. R., REID, I. & FALCONER, R. K. H. 1982. Crustal structure near the Arctic mid-ocean ridge. *Journal of Geophysical Research*, **87**, 1773–1783.

JOLIVET, L., DANIEL, J.-M. & FOURNIER, M. 1991. Geometry and kinematics of ductile extension in alpine Corsica. *Earth and Planetary Science Letters*, **104**, 278–291.

——, ——, TRUFFERT, C. & GOFFÉ, B. 1994. Exhumation of deep crustal metamorphic rocks and crustal extension in arc and back-arc regions. *Lithos*, **33**, 3–30.

KASTENS, K. & MASCLE, J. *ET AL.* 1990. The geological evolution of the Tyrrhenian Sea: an introduction to the scientific results of ODP Leg 107. *In*: KASTENS, K., MASCLE, J. *ET AL.* (eds) *Proceedings of the Ocean Drilling Program, Scientific Results*. College Station, TX (Ocean Drilling Program), **107**, 3–26.

KEEN, C. E. & DE VOOGD, B. 1988. The continent-ocean boundary at the rifted margin off eastern Canada: new results from deep seismic reflection studies. *Tectonics*, **7**, 107–124.

LE DOUARAN, S., BURRUS, J. & AVEDIK, F. 1984. Deep structure of the north-western Mediterranean Basin: Results of a two-ship seismic survey. *Marine Geology*, **55**, 325–345.

LE PICHON, X. 1982. Land-locked oceanic basins and continental collision: the Eastern Mediterranean as a case example. *In*: HSÜ, K. (ed.) *Mountain-Building Processes*. Academic Press, London, 201–211.

—— 1984. The Mediterranean Seas. *In*: *Origin and History of Marginal and Inland Seas*. Proceedings of the 27th International Geological Congress, VNU Science Press, Amsterdam, **23**, 189–222.

—— & ALVAREZ, F. 1984. From stretching to subduction in back-arc regions: dynamic considerations. *Tectonophysics*, **102**, 343–357.

McKENZIE, D. 1978. Some remarks on the development of sedimentary basins. *Earth and Planetary Science Letters*, **40**, 25–32.

—— & BICKLE, M. J. 1988. The volume and composition of melt generated by extension of the lithosphere. *Journal of Petrology*, **29**, 625–679.

MAILLARD, A., MAUFFRET, A., WATTS, A. B., TORNÉ, M., PASCAL, G., BUHL, P. & PINET, B. 1992. Tertiary sedimentary history and structure of the Valencia trough (western Mediterranean). *Tectonophysics*, **203**, 57–75.

MALINVERNO, A. & RYAN, W. B. F. 1986. Extension in the Tyrrhenian Sea and shortening in the Appenines as result of arc migration driven by sinking of the lithosphere. *Tectonics*, **5**, 227–245.

MAUFFRET, A., MAILLARD, A., PASCAL, G., TORNÉ, M., BUHL, P. & PINET, B. 1992. Long-listening multichannel profiles in the Valencia trough (Valsis 2) and the Gulf of Lions (ECORS): a comparison. *Tectonophysics*, **203**, 285–304.

——, PASCAL, G., MAILLARD, A. & GORINI, C. 1995. Tectonics and deep structure of the north-western Mediterranean basin. *Marine and Petroleum Geology*, **12**, 645–666.

MONTIGNY, R., EDEL J.-B. & THUIZAT, R. 1981. Oligo-Miocene rotation of Sardinia : K-Ar ages and paleomagnetism data of tertiary volcanics. *Earth and Planetary Science Letters*, **54**, 261–271.

MOUSSAT, E. 1983. *Evolution de la mer tyrrhénienne centrale et orientale et de ses marges septentrionales en relation avec la néotectonique de l'arc calabrais*. Thèse de 3ème cycle, Université Pierre et Marie Curie, Paris.

NAFE, J.E. & DRAKE, C. L. 1963. Physical properties of marine sediments. *In*: HILL, M.N. (ed.) *The Sea*. Interscience Publishers, **3**, 794–815.

PARKER, R. L. 1973. The rapid calculation of potential anomalies. *Geophysical Journal of the Royal Astronomical Society*, **31**, 447–455.

PASCAL, G., TORNÉ, M., BUHL, P., WATTS A. B. & MAUFFRET, A. 1992. Crustal and velocity structure of the Valencia Trough (Western Mediterranean). Part II: detailed interpretation of five expanded spread profiles. *In*: BANDA, E. & SURINACH, P. (eds) *Geology and Geophysics of the Valencia Trough, Western Mediterranean. Tectonophysics*, **203**, 285–304.

——, MAUFFRET, A. & PATRIAT, P. 1993. The ocean-continent boundary in the Gulf of Lion from analysis of expanding spread profiles and gravity modelling. *Geophysical Journal International*, **113**, 701–726.

PINHEIRO, L. M., WHITMARSH, R. B. & MILES, P. R. 1992. The ocean-continent boundary off the western continental margin of Iberia, II, Crustal structure in the Tagus Abyssal Plain. *Geophysical Journal International*, **109**, 106–124.

RÉHAULT, J.-P. 1981. *Evolution tectonique et sédimentaire du bassin ligure (Méditerranée occidentale)*. Doctorat d'Etat, Université Pierre et Marie Curie, Paris.

——, BOILLOT, G. & MAUFFRET, A. 1984. The Western Mediterranean Basin geological evolution. *Marine Geology*, **55**, 447–477.

——, MOUSSAT, E. & FABBRI, A. 1987. Structural evolution of the tyrrhenian back-arc basin. *Marine Geology*, **74**, 123–150.

——, TISSEAU, C., BRUNET, M.-F. & LOUDEN, K. 1990. Subsidence analysis on the Sardinian margin and the central Tyrrhenian Basin: thermal modelling and heat flow control; deep structure implications. *In*: DANOBEITIA, J. J. & PINET, B. (eds) *Geophysics of the Mediterranean Basin. Journal of Geodynamics*, 269–310.

REID, I. 1994. Crustal structure of a non-volcanic rifted margin east of Newfoundland, *Journal of Geophysical Research*, **99**, 15 161–15 180.

—— & JACKSON, H. R. 1981. Oceanic spreading rate and crustal thickness. *Marine Geophysical Research*, **5**, 165–172.

SANDWELL, D. T. & SMITH, W. H. F. 1995. *Marine Gravity Anomaly from Satellite Altimetry (Map)*. Geological Data Center, Scripps Institution of Oceanography.

SAPIN, M. & HIRN, A. 1974. Results of explosion seismology in the Southern Rhône Valley. *Annales Geophysicae*, **30**, 181–202.

SARTORI, R. 1990. The main results of ODP Leg 107 in the frame of Neogene to Recent geology of Perityrrhenian areas. *In*: KASTENS, K. & MASCLE, J. *ET AL.* (eds) *Proceedings of the ODP, Scientific Results*, **107**, 715–730.

SCOTT, D. R. & STEVENSON, D. J. 1989. A self-consistent model of melting, magma migration and buoyancy-driven circulation beneath mid-ocean ridges. *Journal of Geophysical Research*, **94**, 2973–2988.

SELVAGGI, G. & CHIARABBA, C. 1995. Seismicity and P-wave velocity image of the Southern Tyrrhenian subduction zone. *Geophysical Journal International*, **121**, 818–826.

SPIEGELMAN, M. & MCKENZIE, D. 1987. Simple 2-D models for melt extraction at mid-ocean ridges and island arcs. *Earth and Planetary Science Letters*, **83**, 137–152.

SRIVASTAVA, S. P. & ROEST, W. R. 1995. Nature of thin crust across the southwest Greeland margin and its bearing on the location of the ocean-continent boundary. *In*: BANDA, E., TORNÉ, M. & TALWANI, M. (eds) *Rifted Continent–Ocean Boundaries*. Kluwer Academic Press, Netherlands, 95–120.

STECKLER, M. S. & WATTS, A. B. 1980. The Gulf of Lion: subsidence of a young continental margin. *Nature*, **287**, 425–429.

SU, W., MUTTER, C. Z., MUTTER, J. C. & BUCK, W. R. 1994. Some theoretical predictions on the relationships among spreading rate, mantle temperature, and crustal thickness. *Journal of Geophysical Research*, **99**, 3215–3227.

TALWANI, M. & EWING, M. 1960. Rapid computation of gravitational attraction of three-dimensional bodies of arbitrary shape. *Geophysics*, **25**, 203–225.

TORNÉ, M., PASCAL, G., BUHL, P., WATTS A. B. & MAUFFRET, A. 1992. Crustal and velocity structure of the Valencia trough (western Mediterranean), Part I. A combined refraction/wide-angle reflection and near-vertical reflection study. *Tectonophysics*, **203**, 1–20.

VIALLY, R. & TRÉMOLIÈRES, P. 1996. Geodynamics of the Gulf of Lions. Implications for petroleum exploration. *In*: ZIEGLER, P. A. & HORVÁTH, F. (eds) *Structure and prospects of Alpine basins and forelands*. Peri-Tethys Memoirs, **2**. Edition Technip, Paris, 129–158.

VIGLIOTTI, L. & KENT, D. V. 1990. Paleomagnetic results of Tertiary sediments from Corsica: evidence of post-Eocene rotation. *Physics of the Earth and Planetary Interiors*, **62**, 97–108.

— & LANGENHEIM, V. E. 1995. When did Sardinia stop rotating? New paleomagnetic results. *Terra Nova*, **7**, 424–435.

WATTS, A. B. & TORNÉ, M. 1992*a*. Subsidence history, crustal structure and thermal evolution of the Valencia Trough: a young extensional basin in the Western Mediterranean. *Journal of Geophysical Research*, **97**, 20021–20041.

—— & —— 1992*b*. Crustal structure and the mechanical properties of extended continental lithosphere in the Valencia trough (western Mediterranean). *Journal of the Geological Society of London*, **149**, 813–827.

——, ——, BUHL, P., MAUFFRET, A., PASCAL, G. & PINET, B. 1990. Evidence for reflectors in the lower continental crust before rifting in the Valencia trough. *Nature*, **348**, 631–634.

WESTPHAL, M., ORSINI, J. & VELLUTINI, J. 1976. Le microcontinent corsosarde, sa position initiale: données paléomagnétiques et raccords géologiques. *Tectonophysics*, **30**, 141–157.

WHITE, R. S. & MCKENZIE, D. 1989. Magmatism at rift zones: the generation of volcanic continental margins and flood basalts. *Journal of Geophysical Research*, **94**, 7685–7729.

——, MCKENZIE, D. & O'NIONS, R. K. 1992. Oceanic crustal thickness from seismic measurements and rare earth element inversions. *Journal of Geophysical Research*, **97**, 19 683–19 715.

WHITMARSH, R. B., MILES, P. R. & MAUFFRET, A. 1990. The ocean-continent boundary off the western continental margin of Iberia, I, Crustal structure at 40°30N. *Geophysical Journal International*, **103**, 509–531.

——, PINHEIRO, L. M., MILES, P. R., RECQ, M. & SIBUET, J.-C. 1993. Thin crust at the western Iberia ocean-continent transition and ophiolites. *Tectonics*, **12**, 1230–1239.

ZEYEN, H. J., BANDA, E., GALLART, J. & ANSORGE, J. 1985. A wide angle seismic reconnaissance survey of the crust and upper mantle in the Celtiberian Chain of eastern Spain. *Earth and Planetary Science Letters*, **75**, 393–402.